Resilience Assessment of Tunnel Drop Ceilings Exposed to Blast and Fire

Final Project Report

By

Ziyan Ouyang
Aerik Carlton, Qi Guo
Spencer Quiel

Clay Naito
Email: cjn3@lehigh.edu
Lehigh University

Lehigh University

Sponsorship
U.S. Department of Transportation
Lehigh University Cost Share Support

For

University Transportation Center for
Underground Transportation Infrastructure
(UTC-UTI)

September 2022

Disclaimer

The contents of this report reflect the views of the authors, who are responsible for the facts and the accuracy of the information presented herein. This document is disseminated in the interest of information exchange. The report is funded, partially or entirely, by a grant from the U.S. Department of Transportation's University Transportation Centers Program. However, the U.S. Government assumes no liability for the contents or use thereof.

1. Report No.	2. Government Accession No.	3. Recipient's Catalog No.	
4. Title and Subtitle Resilience Assessment of Tunnel Drop Ceilings Exposed to Blast and Fire		5. Report Date September 2022 6. Performing Organization Code	
7. Author(s) Ziyan Ouyang: https://orcid.org/0000-0003-0629-687X, Aerik Carlton: https://orcid.org/0000-0002-7806-6099, Qi Guo: https://orcid.org/0000-0003-2713-9478, Clay Naito: https://orcid.org/0000-0003-3835-8131, Spencer Quiel: https://orcid.org/0000-0002-1316-7059,		8. Performing Organization Report No.	
9. Performing Organization Name and Address University Transportation Center for Underground Transportation Infrastructure (UTC-UTI) Tier 1 University Transportation Center Colorado School of Mines Coolbaugh 308, 1012 14th St., Golden, CO 80401		10. Work Unit No. (TRAIS) 11. Contract or Grant No.	
12. Sponsoring Agency Name and Address United States of America Department of Transportation Research and Innovative Technology Administration		13. Type of Report and Period Covered Final Report (Sept. 2016 to Oct. 2018) 14. Sponsoring Agency Code	
15. Supplementary Notes Report also available at: https://zenodo.org/communities/utc-uti			
16. Abstract Tunnels are critical links within modern transportation networks and are susceptible to accidental explosion and fire from vehicle fuel and cargo. They also present a target for terrorism due to unscreened public access. Roadway tunnels constructed with circular, oval, or horseshoe cross-sections in the United States within the last 100 years have typically consisted of a road surface, tunnel liner, and drop ceiling. The drop ceiling is hung from the liner and creates a plenum above the roadway for ventilation of vehicle exhaust as well as throughput for electrical conduit, utilities, fire alarms, and fire suppression systems. Drop ceiling panels are lightweight relative to the much thicker tunnel liner and can experience significant damage due to a fire or blast event on the roadway below. Two studies are conducted on prototype drop ceiling systems examining bot the resistance to blast and fire events. The studies examine the likelihood of significant damage and collapse of tunnel drop ceilings. Six blast scenarios consisting of three TNT charge sizes in two representative tunnels were analyzed using computational fluid dynamics (CFD) to generate blast demands on the drop ceiling, followed by a blast vulnerability assessment of the drop ceiling panels. The results illustrate that modestly sized explosive hazards can induce significant damage ranging from permanent deformation up to widespread collapse. Retrofit options include hardening via flexural enhancement with FRP as well as retrofit of the hangers; however, removal of the ceiling and reconfiguring the ventilation system with modern jet fans may be a more cost-effective option for blast mitigation. The systems are also evaluated to assess performance under fire events. Standard fire demands per the RWS and ASTM E1529 fire curves are uniformly applied to the ceiling panels, while the heat exposure contours for typical vehicle fires with heat release rates of 30 MW, 100 MW, and 200 MW are generated from the software CFAST. The analysis results indicate that drop ceiling panels are highly vulnerable to fire-induced damage and potential collapse. Fire-induced damage can be mitigated by reducing the fire hazard, removing the drop ceiling, or enhancing the fire resistance of the panels via the application of passive protection or structural hardening.			
17. Key Words Tunnel Drop Ceilings, Explosion, Blast, Concrete, Fire, Tunnel		18. Distribution Statement No restrictions.	
19. Security Classification (of this report) Unclassified	20. Security Classification (of this page) Unclassified	21. No of Pages 99	22. Price NA

Table of Contents

List of Figures

List of Tables

List of Abbreviations

ACI: American Concrete Institute

ASCE: American Society of Civil Engineers

ASTM: American Society for Testing and Materials

CFAST: Consolidated Fire and Smoke Transport

CFD: Computational Fluid Dynamics

DOT: Department of Transportation

FEM: Finite Element Method

FRP: Fiber Reinforced Polymer

HRR: Heat Release Rate

NFPA: National Fire Protection Association

RWS: Rijkswaterstaat

SDOF: Single Degree of Freedom

TNT: Trinitrotoluene

USD: United States Dollar

Executive Summary

Tunnels are critical links within modern transportation networks and are susceptible to accidental explosion and fire from vehicle fuel and cargo. They also present a target for terrorism due to unscreened public access. Roadway tunnels constructed with circular, oval, or horseshoe cross-sections in the United States within the last 100 years have typically consisted of a road surface, tunnel liner, and drop ceiling. The tunnel liner is the main structural component that resists any over-tunnel loads as well as preventing substrate intrusion and cave-ins. The drop ceiling is hung from the liner and creates a plenum above the roadway for ventilation of vehicle exhaust as well as throughput for electrical conduit, utilities, fire alarms, and fire suppression systems. Drop ceiling panels are lightweight relative to the much thicker tunnel liner and can experience significant damage due to a fire or blast event on the roadway below, for the typical design of a tunnel drop ceiling only considers gravity loading and forces exerted by pressure within the ventilation plenum at room temperature therefore presents significant risk of drop ceiling damage or collapse.

This study first illustrates the likelihood of significant damage and collapse of tunnel drop ceilings under blast loading. Six scenarios consisting of three TNT charge sizes in two representative tunnels were analyzed using computational fluid dynamics (CFD) to generate blast demands on the drop ceiling, followed by a blast vulnerability assessment of the drop ceiling panels. Single Degree of Freedom (SDOF) dynamic analyses are verified against finite element method (FEM) solutions and used to evaluate the damage inflicted for a wide range of blast demands. The study then examines the flexural response of drop ceiling panels in two representative tunnels to standard fire curves as well as several realistic fires due to vehicular accidents. Standard fire demands per the RWS and ASTM E1529 fire curves are uniformly applied to the ceiling panels, while the heat exposure contours for typical vehicle fires with heat release rates of 30 MW, 100 MW, and 200 MW are generated from the software CFAST. The finite element analysis software SAFIR is used to evaluate the thermo-mechanical behavior of the ceiling panels when subjected to various thermal demands from the fire below.

Findings

Modestly sized explosive hazards can induce significant damage ranging from permanent deformation up to widespread collapse. Retrofit options to improve blast performance of tunnel drop ceilings include hardening via flexural enhancement with FRP as well as retrofit of the hangers; however, removal of the ceiling and reconfiguring the ventilation system with modern jet fans may be a more cost-effective option for blast mitigation. Drop ceiling panels are also highly vulnerable to fire-induced damage and potential collapse both during a fire's active heating phase (from simultaneous loss of capacity and restraint of thermal expansion) and during the subsequent cooling period (due to tension that develops when the permanently deformed panel thermally retracts). The potential for fire-induced damage or collapse of the drop ceiling panels can be mitigated by reducing the fire hazard, removing the drop ceiling, or enhancing the fire resistance of the panels via the application of passive protection or structural hardening.

Chapter 1: Project Scope

In Years 1 through 3, researchers at Lehigh University developed a new framework for evaluating the vulnerability of tunnel infrastructure to blast and fire hazards. The effort focused on the spatial and temporal distribution of the loading effects due to blast and fire. Specifically, two journal papers have been submitted (one published and the other with revisions under review) which proposed fast-running and conservatively accurate models which calculate the blast-induced loading as well as fire-induced heat flux exposure for a range of relevant threats.

This report extends the tool to include structural damage and resulting functionality consequences due to the mapped exposure for blast hazards. Specifically, evaluation of drop ceiling structures that are commonly installed in tunnels to separate the main shaft from ventilation and other mechanical systems are examined. The resulting assessments are used to prioritize and tailor mitigation strategies, systems, and placement to maximize risk reduction with available resources. High fidelity modeling will be used to validate the fast-running analytical models and quantify the associated damage and the potential for progressive structural damage as well as down-time and economic costs.

Chapter 2: Introduction and Background

Tunnels are a critical component of modern transportation infrastructure that provide efficient movement of goods and people under difficult terrain, waterways, and dense urban areas. Reduction in tunnel functionality due to closure of a single lane or an entire bore can lead to significant economic losses at local, regional, and national levels. For example, the 1999 fire in the Mont Blanc tunnel between Italy and France resulted in an estimated $267 million USD of repair costs; however, the estimated business interruption loss (including losses in both countries) due to just a few months of reduced functionality exceeded the tunnel repair costs at $287 million USD (*1*).

A drop ceiling (also known as hanging, suspended, or false ceiling) is a common construction feature for roadway tunnels that have a circular, oval, or horseshoe cross-section. Numerous roadway tunnel designs going back to the 1927 construction of the Holland Tunnel have incorporated plenums above and/or below the roadway surface. These plenums are primarily used to supply fresh air and remove vehicle exhaust, particularly carbon monoxide. A plenum above the roadway is constructed using a drop ceiling of thin reinforced concrete panels, which are typically precast and then installed within the tunnel liner using doweled wet connections and tension hangers. Ceiling plenums in modern tunnels can also house utility conduits, provide support for lighting and active fire prevention systems, and ventilate smoke and hot gas during fire events. Fig. 1 illustrates the basic elements of a generic tunnel equipped with a drop ceiling. The life safety design requirements of NFPA 502 (*11*) and the resulting need to achieve critical air velocity for longitudinal tunnel ventilation has led to an increased use of jet fans or Saccardo nozzles that are mounted to the tunnel liner (*12*). These systems have higher ventilation capacity than transverse and semi-transverse systems that utilize partitioned plenums for air supply and removal. Longitudinal ventilation systems have become increasingly prevalent in new tunnel construction and have enabled the elimination of ceiling panel plenums in numerous existing tunnels; however, a large proportion of existing U.S. tunnels still utilize plenums with drop ceilings. Typical drop ceilings are constructed of thin precast reinforced concrete panels that are doweled into the tunnel liner at shelf supports on either end of the tunnel width (i.e. perpendicular to the longitudinal direction of traffic flow) and supported vertically by tension hangers at one or more locations along the tunnel width. The ceiling hangers are connected to the panel by various types of embedded steel anchorages and extend vertically to embedded or post-installed anchorages in the tunnel liner above.

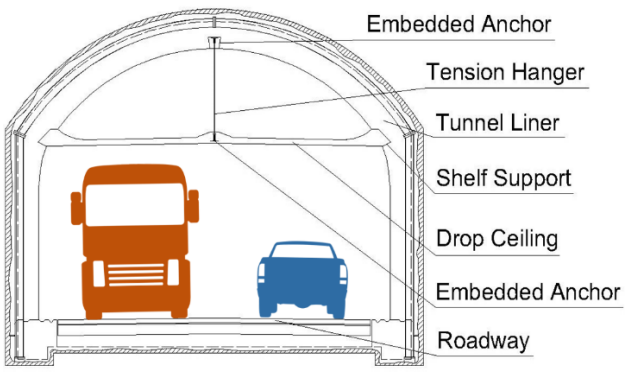

Fig. 1: Representative tunnel with a drop ceiling in a horseshoe cross-section

Fig. 2 plots the United States roadway tunnel inventory from 1865 to 2017 (with approximately 503 roadway tunnels currently identified as active) according to cross-sectional type as defined by the US Department of Transportation (*2*). Based on limited data provided in that database as well as a visual review of each tunnel using Google Maps Street View in May 2019 (*3*), the number of tunnels with drop ceilings are estimated and plotted against the national tunnel inventory in Fig. 2. The results show an increase in utilization of drop ceilings starting in the mid-twentieth century. In recent decades, the drop ceilings in some tunnels have been removed, with legacy ventilation systems subsequently replaced by jet fans (for example, the 2004 Squirrel Hill Tunnel ceiling removal near Pittsburgh, PA (*4*)). Approximately 94 tunnels (or 19% of the total tunnel inventory) are currently or were once equipped with drop ceilings. Since most tunnels equipped with drop ceilings are highway tunnels, the lengths of these tunnels are relatively long compared to those without drop ceilings. The total length of tunnels with drop ceilings is estimated to be 48% of the total U.S. tunnel length (i.e. 96 km of the 200-km total). Moreover, these tunnels are typically utilized for roadways with larger traffic volumes, which can result in significant economic consequences due to any disruption of functionality.

Failure and subsequent collapse of drop ceiling panels poses a significant fall hazard to vehicles below as well as substantial losses of tunnel functionality. For example, the 2006 collapse of a ceiling panel in Boston's Fort Point Channel Tunnel due to the failure of an epoxy concrete anchor resulted in several casualties (including 1 fatality), closure of the tunnel for over a year, and $54M USD in additional costs to redesign, inspect, and repair the tunnel (*5*). A similar failure in 2012 of more than 300 panels in Tokyo's Sasago Tunnel (*6*) due to anchorage deterioration caused nine fatalities as vehicles below were crushed during the collapse. That oval-shaped tunnel was subsequently closed for more than a month for extensive removal and repair of the drop ceiling.

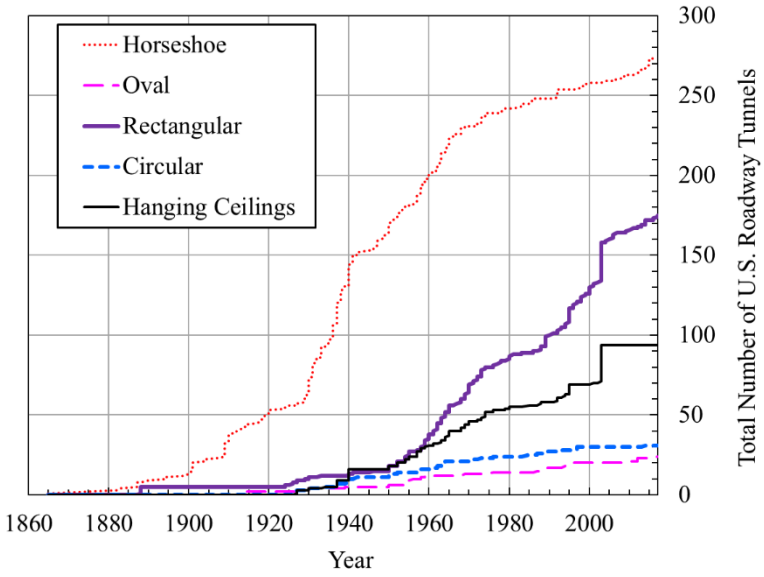

Fig. 2: United States roadway tunnel inventory from 1865 to 2017

Though a low probability event, confined explosions within a tunnel can pose an even greater potential for structural component damage or collapse of tunnel systems. Tunnels are susceptible to explosive blast loads due to accidental detonation of vehicle fuel (e.g., hydrocarbon, hydrogen, or batteries), vehicle-borne cargo, or intentional detonations due to terrorism (since they are high-value assets and publicly accessible to wide ranges of traffic). For example, the 1969 gas explosion

in the abandoned tunnel underneath Delancey Street in Manhattan, NY resulted in severe damage to the tunnel and pavement buckling on the surface street above for over four city blocks. The subway lines and stations nearby were disrupted as well as street traffic, which forced the closure of the westbound lane of the Williamsburg Bridge (*7*). Despite this, a relatively large explosive threat (typically quantified in terms of equivalent weight of TNT) is needed to significantly damage the reinforced concrete liner in most roadway tunnels. A recent study by the authors indicated that hazards greater than 226.8 kg (500 lbs) of TNT would be needed to inflict significant spall damage, and hazards ranging from 453.6 kg (1000 lbs) to 907.2 kg (2000 lbs) would be needed to significantly breach the reinforced concrete liner of a typical roadway tunnel (*8*). These hazards are associated with large trucks and represent the higher end of threat sizes that are considered for blast hazard threat assessment of transportation assets (*9*).

Tunnel liners have significant blast resistance due to their significant thickness and mass, and most are continuously backed by the surrounding media (consisting of soil, rock, and grout). Drop ceiling panels, on the other hand, are designed to be thin to reduce self-weight as they separate the main passageway from the plenum above – because they are unbacked, these panels responding in flexure and shear when subjected to blast demands from within the tunnel. Tunnel drop ceilings are typically designed only for gravity and service loads, whereas explosions on the roadway below produce upward pressure on the drop ceiling. This impulsive uplift can result in significant damage at relatively modest blast intensities that are well below that needed to damage the liner. For example, the blast hazard potential of conventional and alternative fuel vehicles themselves (*10*) or hazardous cargo with explosive potential much less than 226.8 kg (500 lbs) of TNT could cause significant damage to these drop ceiling systems.

According to data from National Highway Traffic Safety Administration, the number of annual car crashes in the U.S. is trending upward, from 5.4 million crashes reported in 2010 to 6.4 million crashes reported in 2017 (*14*). With greater crash risk comes a higher likelihood of a subsequent fire, the severity of which will depend on the vehicles involved (*11*, *15*). Roadway tunnels have an extensive history of fire events which have resulted in damage severities ranging from limited non-structural effects to severe structural damage, including individual element collapse in some of the worst cases (*16*). The constant presence of moving vehicles carrying combustible and/or hazardous materials (both vehicle fuel and cargo) through an enclosed environment makes tunnels susceptible to severe fire events (*15*). As such, tunnels are often more vulnerable to fire compared to other highway structures such as bridges, which are typically subjected to open-air fire hazards (*17*). Reduction in tunnel functionality due to closure of a single lane or an entire bore can lead to significant economic losses, and the collapse of any tunnel components during or after a fire will pose a direct threat to user life safety. Furthermore, even if tunnel components such as drop ceilings survive a fire event, the possible long-term impacts to tunnel safety due to a permanent loss of their capacity or durability should also be considered for subsequent maintenance, inspection, and repair.

Tunnel liners have significant fire resistance due to their substantial thickness, and most are continuously backed by the surrounding media (consisting of soil, rock, and grout). Fire-induced damage to the concrete tunnel liner typically consists of spalling, micro-cracking, and an associated decrease in surface strength and stiffness. Drop ceiling panels, on the other hand, have relatively long spans between supports and are designed to be relatively thin to minimize their self-weight. These panels therefore respond in flexure when subjected to fire demands from the roadway below (*13*).

While explosions are a low-probability event, the potential for high consequence via drop ceiling collapse therefore creates a tangible risk for most tunnels. This study firstly evaluates the resilience of drop ceiling systems in tunnels to explosion-induced damage by quantifying the explosive threat, obtaining the resulting spatial and temporal distribution of blast pressure demands within a typical tunnel, assessing structural resistance of the drop ceiling panels, and determining expected extents and severity of damage. The performance of drop ceiling systems in two realistic tunnels are examined in this study for a range of blast threat sizes. Mitigation strategies with associated cost-benefit are also presented. After the evaluation of blast vulnerability, the performance of conventional drop ceilings is examined numerically using standard fire exposure curves as well as thermal demands from simulated vehicle fire events, which illustrate the effect of realistic heat distribution on the structural behavior of the panel. The sizes of the realistic fire events are selected based on a recently completed stochastic study of thermal demands from vehicle fires, which summarizes the cumulative frequency distribution for potential heat release rates (HRRs) in the Fort Pitt Tunnel near Pittsburgh, PA (*15*). Per NFPA 502, the HRR of fire events from heavy goods vehicles (HGV) can range from 20 to 200 MW (*11*). To address the potential damage from a relatively low-probability event, several fire sizes within the NPFA 502 HGV range are utilized for thermal evaluation of drop ceiling systems in two representative tunnels. The during-fire and post-fire vulnerability of drop ceiling systems in these tunnels are evaluated via nonlinear thermo-mechanical analysis of the reinforced concrete panels, and mitigation strategies are subsequently discussed to provide guidance for future tunnel construction and rehabilitation.

Chapter 3: Case Study of Tunnel Drop Ceilings Exposed to Blast

This case study will present the likelihood of damage from low to high level and potential collapse of tunnel drop ceilings in the aftermath of a blast event. Two representative tunnels with two-lane and three-lane traffic were analyzed. For each tunnel, three TNT charge sizes were analyzed using computational fluid dynamics (CFD) to generate blast demands on the drop ceiling, followed by a blast vulnerability assessment of the drop ceiling panels. Single Degree of Freedom (SDOF) dynamic analyses are verified against finite element method (FEM) solutions and used to evaluate the damage inflicted for a wide range of blast demands.

3.1 Prototype Tunnel Details

To illustrate the potential severity and extent of damage in the aftermath of an explosive event, two representative tunnels with drop ceilings are subjected to a range of explosive charge sizes. The tunnel details were provided by state departments of transportation (DOTs) in the US and represent systems that are currently in service. Tunnel 1 was built in 1970 and supports three lanes of traffic. Tunnel 2 was built in 1960 and supports two lanes of traffic. Both tunnels have horseshoe-shaped cross-sections (the most common shape as shown in Fig. 2) and support relatively high volumes of highway traffic (over 100,000 vehicles per day). Three charge sizes of equivalent TNT [22.7 kg (50 lbs), 45.4 kg (100 lbs) and 226.8 kg (500 lbs)] were selected to characterize a range of hazards that could be associated with an accidental blast.

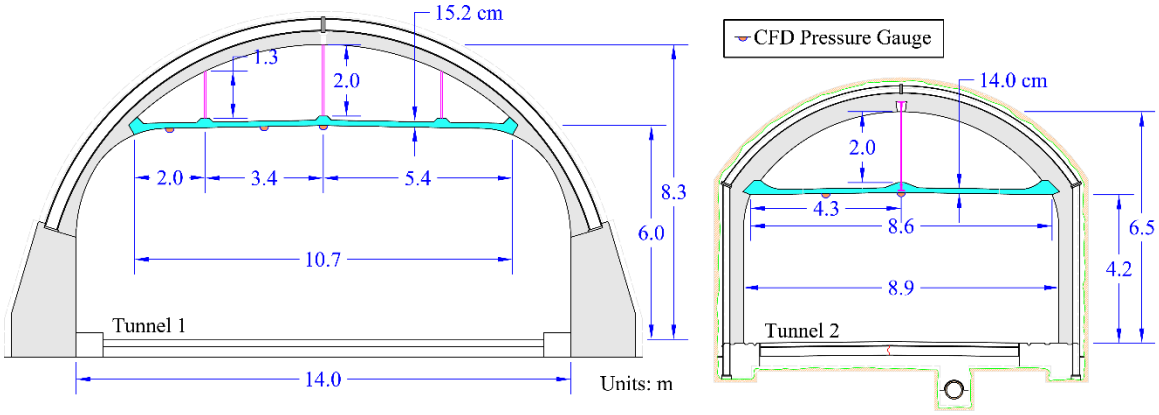

Fig. 3: Prototype tunnel cross-sections (units in meters)

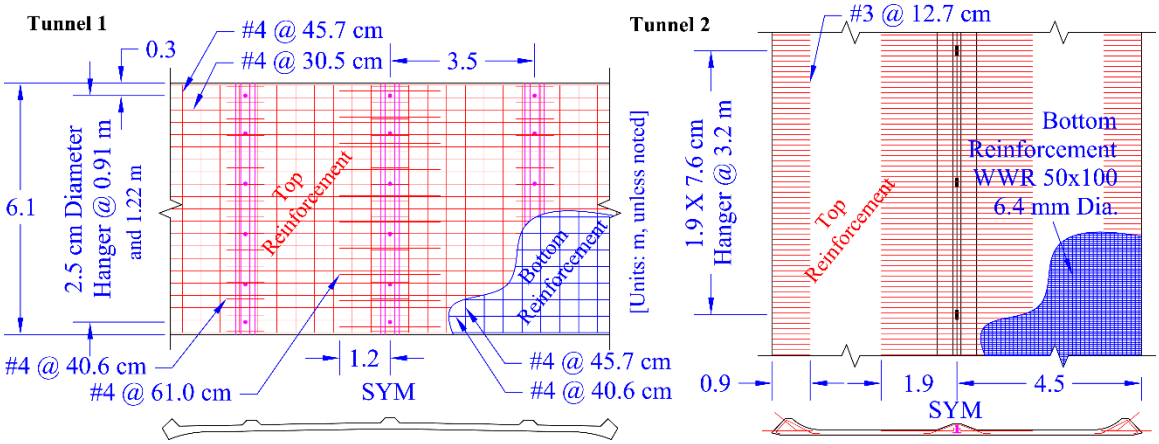

Fig. 4: Plan of ceiling panel reinforcement

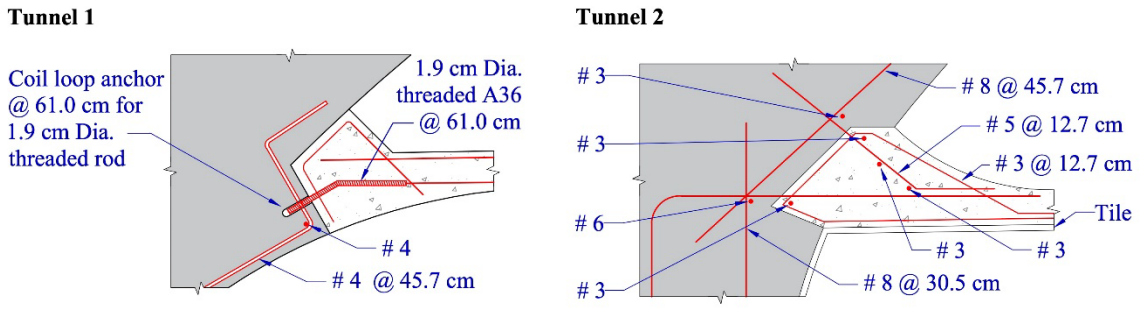

Fig. 5: Detailing at the interface of the ceiling panel and tunnel liner

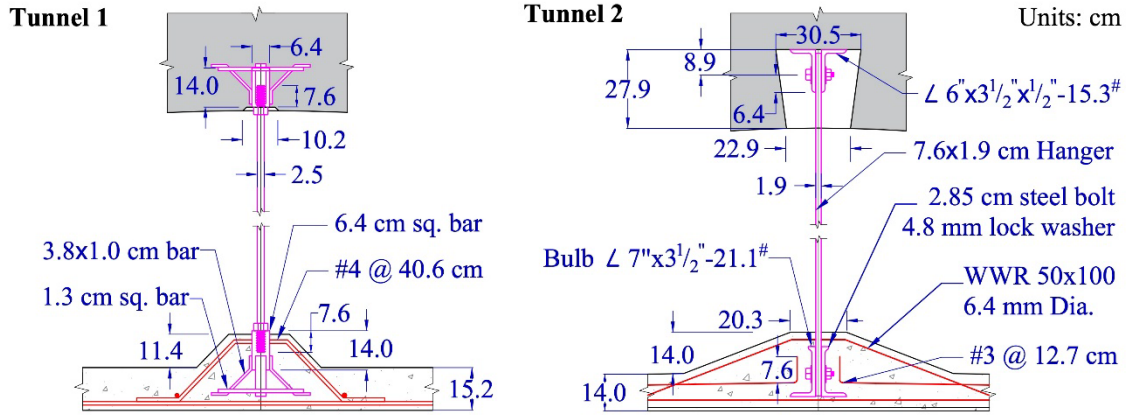

Fig. 6: Details of the hanger between the tunnel liner and ceiling panels

The two representative roadway tunnels are illustrated in Fig. 3 and Fig. 4. Tunnel 1 is approximately 305 m (1000 ft) in length. The drop ceiling has a total transverse span of 11.0 m (36 ft) and is longitudinally panelized into 6.1 m (20 ft) segments. Each panel is supported by shelf supports at its ends (Fig. 5) and 18 tension hangers (Fig. 6). Six rows of hangers are used in the roadway direction with three hangers in the transverse direction (Fig. 4). Each hanger has an assumed nominal yield strength of 276 MPa (40 ksi) (ASCE/SEI 2014). The interface between the ceiling panels and the shelf supports consist of a coil anchor and threaded rod (see Fig. 5). Since this interface lacks moment-resisting design elements, it is assumed to be rotationally flexible. The ceiling panels are designed with continuous top and bottom reinforcing steel as shown in Fig. 4.

Tunnel 2 is approximately 1100 m (3600 ft) in length and is smaller in width and height than Tunnel 1. Due to confinement effects, the blast-induced demands and subsequent response of the structure will differ from Tunnel 1 due to the reduced free volume and distance (i.e. standoff) from the explosive hazard to the liner and ceiling. The ceiling has a total transverse span of 8.6 m (28 ft – 1 in.) and is longitudinally panelized into 15.3-m (50 ft – 4 in.) segments. Each panel is supported at midspan by three tension hangers (see Fig. 4 and Fig. 6) that are spaced at 3.2 m (10 ft – 6 in.), again with an assumed nominal yield strength of 276 MPa (40 ksi) (ASCE/SEI 2014). The edges of the ceiling panels (parallel to the tunnel direction) are heavily doweled into the liner, resulting in relative rotational fixity at the supports as shown in Fig. 5. Unlike Tunnel 1, Fig. 4 shows that the top reinforcement in Tunnel 2 is discontinuous at over the middle half of the span between the edge support and tension hanger, resulting in a relatively low resistance against upward flexural demands. Both ceiling systems are analyzed as one-way elements with the primary longitudinal

reinforcement located 25 mm (1 in.) from each surface. Transverse reinforcement is located between the two layers of longitudinal bars.

3.2 Blast Demand Evaluation

An explosive event in a tunnel will be partially confined due to its tubular construction. The level of confinement is dependent on the location of the detonation relative to the open ends of the tunnel as well as the tunnel's overall length. For simplification, the case study in this paper assumes that the explosive hazard is located at the longitudinal and transverse center of each tunnel, which results in upper-bound confinement for detonation. The pressure time histories for each combination of hazard size and tunnel geometry are determined via computational fluid dynamics (CFD) modeling in ProSAir (*19*), which was developed at Cranfield University to assess blast wave propagation within complex physical spaces such as cityscapes, confined geometries, and vented compartments. ProSAir has been previously validated by its developers via comparisons with ConWep (*20*) and AUTODYN-3D (*21*) against the Swisdak dataset as well as for a 1/10th scale model of the Whalen experiments (Rose 2010). Typically, ProSAir is referenced as a CFD equivalent of LS-DYNA (*23*), VAPO (*24*), and BlastX (*25*, *26*), and it has been shown to be less computationally expensive compared to AUTODYN-3D (Rose 2010).

The ProSAir models developed for this study assume initial ambient atmospheric conditions within the tunnel with pressure equal to 101.3 kPa (14.7 psi) and temperature of 284 K (51.5ºF). The explosive threat is placed 0.6 m (2.0 ft) above the roadway surface to approximate the ground clearance of a vehicle. When each analysis is initiated, the computations of blast-induced shock wave propagation are made using spherical coordinates until the first boundary surface of the tunnel structure is met by the blast wave. Spherical computations are completed using polar coordinate cells that are discretized to 0.38 cm (0.15 in.) radial increments. Once the blast wave makes first contact with a physical surface, the analysis then engages the user-defined 3D volume (which is discretized for these prototype tunnels into rectangular cells with a 15.2 cm (6.0 in.) maximum edge dimension) for the remainder of the simulation. The full length of the tunnel is modeled to allow the blast wave propagation and its internal reflections to reach the openings at either end, and the computational duration was iteratively tailored such that the blast wave reached the openings by the end of the analysis. In the 3D model geometry, the tunnel liner, roadway surface, and drop-ceiling were modeled as fully reflective (i.e. non-frangible) rigid obstructions. Even though the drop ceiling panels will be damaged by the blast wave, this assumption produces conservative blast demand output by inducing maximum (i.e. worst-case) blast wave reflection within the tunnel. A sample CFD pressure distribution from one of the ProSAir analyses is illustrated in Fig. 7.

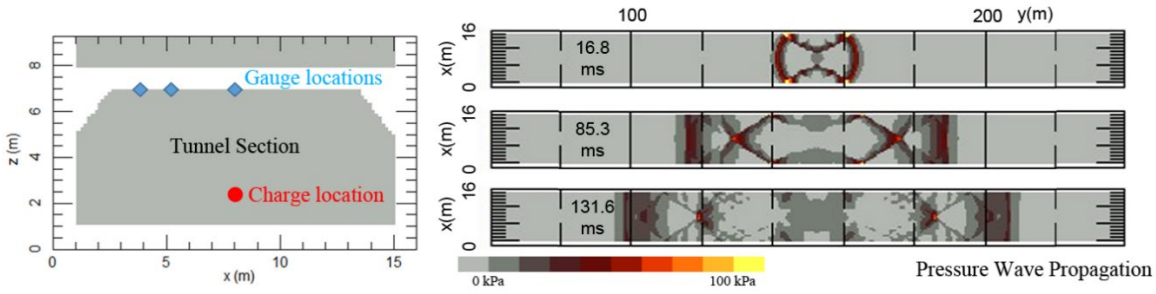

Fig. 7: Representative visualization of ProSAir CFD results for Tunnel 1

Pressure gauges are placed in the model at locations of interest along the transverse span of each panel and at regular locations along the length of the tunnel. Figs. 3 and 7 show the gauge locations on the cross-sections of the tunnel ceilings. Each gauge records the pressure time history – Fig. 8, for example, shows the pressure time histories along the ceiling of Tunnel 1 for the 226.8 kg (500 lbs) charge size at three longitudinal distances from the detonation location along the middle of the tunnel. Note that the pressure axis for each time history in Fig. 8 has been normalized to the peak pressure at that location in order to compare their shape, as locations closer to the detonation will experience considerably higher peak pressure.

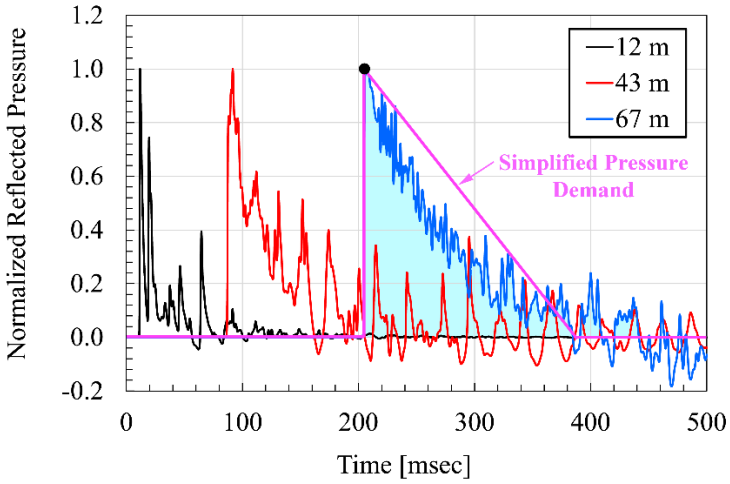

Fig. 8: Normalized pressure time histories at several longitudinal distances from the charge location

The pressure time history demands at each gauge can be used as blast load input for subsequent dynamic analysis of the drop ceiling panels. As is typically done in industry practice, each time history is simplified as an equivalent triangular ramp-down loading function (*27*, *28*). In general, the pressure rises to the peak value almost instantaneously and decays more slowly due to confinement effects, which can be reasonably approximated as a ramp-down right triangle. The peak pressure from the ProSAir simulation is set as the height of the triangular load, and the equivalent time duration is calculated such that the area under the triangular loading function is equal to that under the ProSAir pressure time history (i.e. both the equivalent and ProSAir time histories will generate the same impulse). Typical blast resistant design approaches will conservatively neglect the negative phase of the pressure time history (which would slightly mitigate the effects of the positive phase) – this study likewise neglects the negative phase when evaluating the ceiling panel response.

An example triangular time history simplification is shown in Fig. 8 for the case of the blast demand at 67 m (220 ft) from the threat location. Note that some locations along the tunnel length will experience a pressure time history that does not fit the triangular ramp-down load simplification shown in Fig. 8 – in those cases, the peak pressure may occur later in the time history due to internal reflections within the tunnel. However, dynamic analysis of the drop ceiling panels using an ill-fitting triangular time history in these limited cases will induce a more significant structural response than the time history loads from ProSAir by delivering a more consolidated impulse of pressure loading. The triangular simplification is therefore considered to be an

acceptably conservative approximation of the pressure time histories from ProSair and is used for all structural analysis of the drop ceiling panels in this study.

Table 1: Summary of Maximum and Minimum Pressure and Impulse

Tunnel	Charge Size kg (lbs)	Max. Pressure kPa (ksi)	Max. Impulse kPa-ms (ksi-ms)	Min. Pressure kPa (ksi)	Min. Impulse kPa-ms (ksi-ms)
Tunnel 1	226.8 (500)	8008 (1162)	13175 (1911)	71 (10)	4904 (711)
	45.4 (100)	1073 (156)	2867 (416)	28 (4)	1106 (160)
	22.7 (50)	366 (53)	1236 (179)	19 (3)	636 (92)
Tunnel 2	226.8 (500)	14609 (2119)	20939 (3037)	56 (8)	10814 (1569)
	45.4 (100)	3516 (510)	5926 (859)	23 (3)	2380 (345)
	22.7 (50)	1388 (201)	2857 (414)	15 (2)	1345 (195)

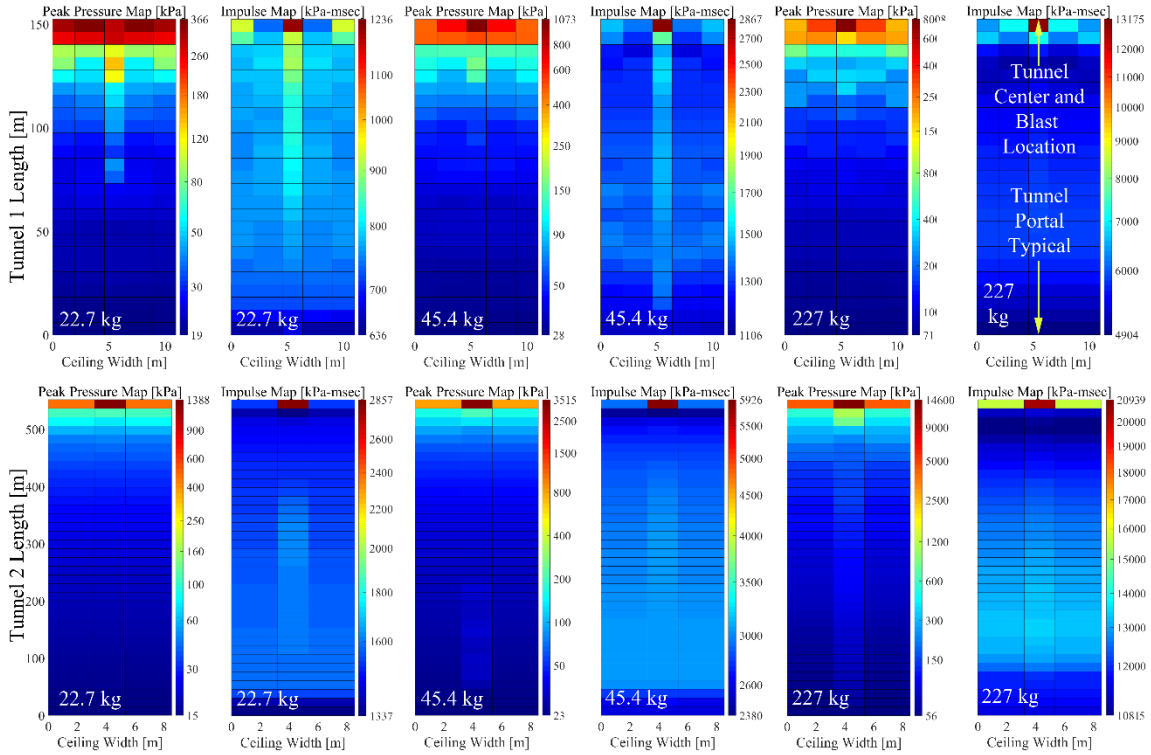

Fig. 9: Maps of pressure and impulse demands on the tunnel ceilings due to each threat size

Fig. 9 maps the peak reflected pressure and impulse from ProSAir onto the ceiling segments along half the length of each tunnel due to each blast threat (which is located in plan at the top center of each plot). Table 1 summarizes the maximum and minimum recorded values of pressure and impulse among all locations in the two prototype tunnels for the three charge sizes. As expected, there is a significant reduction in peak overpressure and impulse at increased standoff from the charge location, with the peak demands occurring directly overhead. As the charges were placed 0.6 m (2 ft) above the roadway surface, the minimum standoff distances from the charge to the

drop ceiling of Tunnel 1 and Tunnel 2 are therefore 5.3 m (17.3 ft) and 3.7 m (12.0 ft), respectively. As shown in Table 1, Tunnel 2 experiences a significantly higher blast demand for the same charge size versus Tunnel 1 due to the lower ceiling height. Ceiling clearance therefore plays a large role in determining the potential for blast-induced structural damage to drop ceiling systems.

3.3 Structural Resistance Assessment

The blast vulnerability of the drop ceilings is assessed by determining the structural resistance of the panel, which is then used to calculate the damage corresponding to various combinations of pressure and impulse. As shown in Fig. 10, each ceiling panel in the two tunnels is a multi-span flexural component due to the presence of the ceiling hangers. The slender hangers have low compressive resistance and can buckle when subjected to upward blast load reactions. If the hangers buckle right after blast loading is applied, the panel would be analyzed as a single span between the ends supports at the tunnel liner (i.e. Cases A and B for Tunnel 1, and Cases I and II for Tunnel 2 in Fig. 10). If the hangers are not immediately overloaded, they can provide some support reaction and induce multi-span flexural behavior (i.e. Cases C and D for Tunnel 1, and Cases III and IV for Tunnel 2 in Fig. 10).

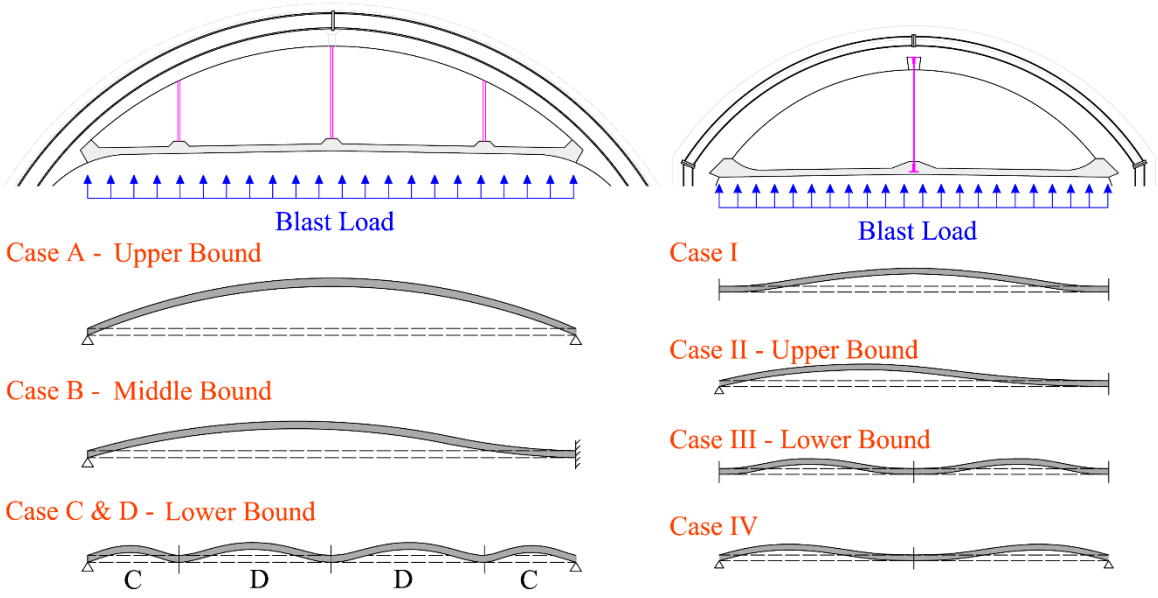

Fig. 10: Idealized boundary conditions for prototype ceiling panels

As shown previously in Fig. 5, the interface of the panel at its support on the tunnel liner is realistically semi-rigid, with the Tunnel 1 panels having more rotational flexibility due to less anchorage reinforcement than those in Tunnel 2. Both pinned and fixed boundary conditions are therefore considered to bracket the behavior of the actual interface connections.

Table 2 summarizes the boundary conditions of each panel span analysis case. Tunnel 1 is analyzed with pin-pin (Case A) and pin-fix (Case B) end conditions for the single span cases due to the higher rotational flexibility of the coil anchor at its liner interface. The multi-span Cases C and D are analyzed only with the lower bound pinned ends at the liner interface, and the continuous boundaries between spans are approximated as rotationally fixed. Tunnel 2 is analyzed with pin-fix (Case I) and fix-fix (Case II) end conditions since it has doweled reinforcement at the liner interface. The multi-span Cases III and IV are modeled with fixed and pinned ends, respectively; the continuous boundaries between spans are again approximated as rotationally fixed.

Table 2: Panel span conditions for structural analysis

Tunnel	Panel Thickness	Shear Capacity	Case	Length of Span	Boundary condition
Tunnel 1	12.7 cm (5.0 in)	104.6 kN/m (7.2 kip/ft)	Case A	11.0 m (36.0 ft)	pin-pin
			Case B	11.0 m (36.0 ft)	pin-fix
			Case C	2.0 m (6.5 ft)	pin-fix
			Case D	3.5 m (11.5 ft)	fix-fix
Tunnel 2	15.2 cm (6.0 in)	83.7 kN/m (5.7 kip/ft)	Case I	8.5 m (28.0 ft)	fix-fix
			Case II	8.5 m (28.0 ft)	pin-fix
			Case III	4.3 m (14.0 ft)	fix-fix
			Case IV	4.3 m (14.0 ft)	pin-fix

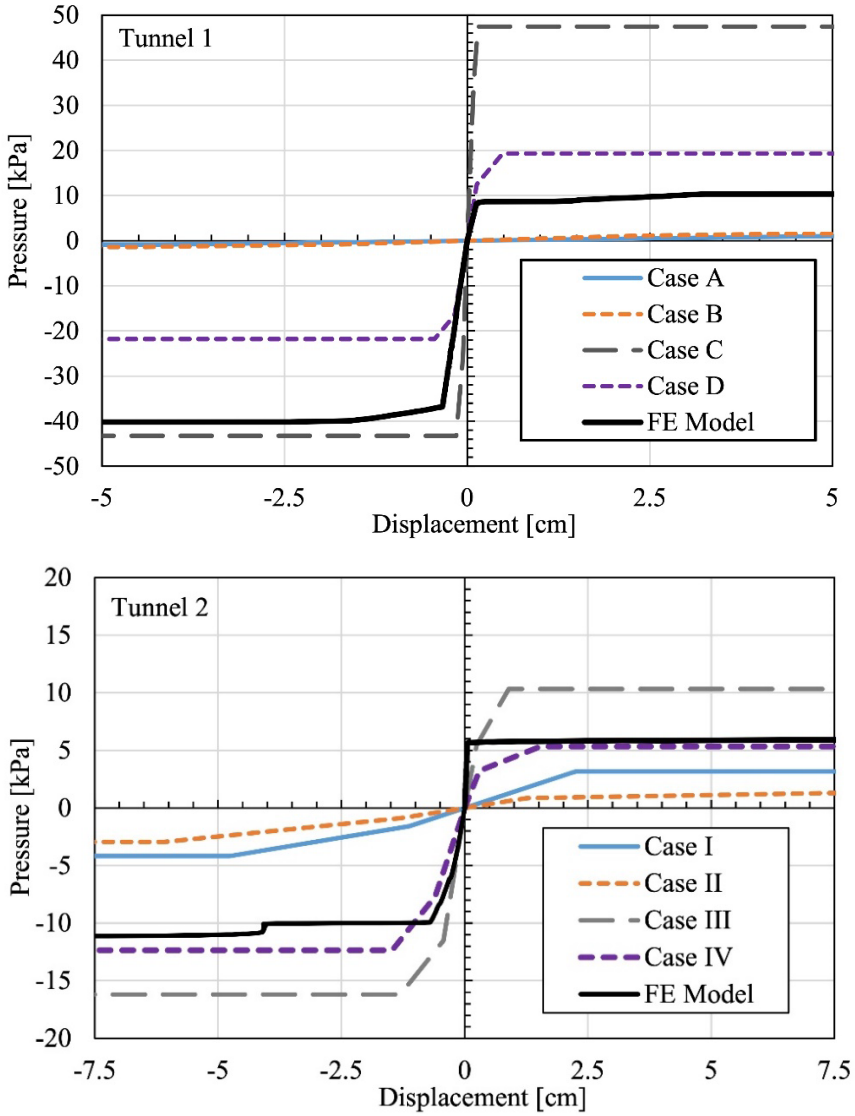

Fig. 11: Flexural resistance functions for simplified and FE ceiling panel models

The flexural resistance function and nominal shear capacity for each ceiling panel span (summarized in Table 2) are determined in accordance with simplified procedures for reinforced concrete members subject to flexural response per UFC 3-340-02 (*29*) and ACI 318-19 (ACI Committee 318 2019). The thickness used in the analyses of each panel is based on the minimum thickness shown previously in Fig. 3. Based on the age of the systems and their design drawings, the compressive strength of the concrete was conservatively assumed to be 20.7 MPa (3000 psi), and the steel reinforcement was assumed to have a nominal yield strength of 276 MPa (40 ksi) (ASCE/SEI 2014). The stress-strain behavior of the reinforcement was idealized as elastic-perfectly-plastic (i.e. strain hardening is conservatively neglected), and concrete tensile strength is also neglected. To account for high strain rate effects, dynamic increase factors of 1.19 and 1.17 are applied to the concrete compressive strength and reinforcement yield strength, respectively. These increase factors represent the standard values used for dynamic response of reinforced concrete components in flexure per UFC 3-340-02 (*29*). The resistance in both the inbound (positive upward) and rebound (negative downward) directions are computed to account for variations in top and bottom reinforcement as shown previously in Fig. 4. The resistance functions for all simplified span cases of both tunnels due to uniform pressure loading are plotted in Fig. 11. As expected, the single span cases where the hangers buckle immediately (e.g., Cases A, B, I, and II) result in a much lower resistance due to the larger effective span. Note that the blast response is primarily controlled by the initial inbound loading; however, both the rebound and inbound resistance are developed in order to calculate a complete blast-induced response.

To verify the simplifying assumptions that were used to derive these resistance functions, the ceiling panels were numerically modeled via explicit finite element (FE) analysis in Abaqus/CAE 2018 (*31*). A three-dimensional model of a tributary section of each ceiling panel was constructed using rectangular S4R shell elements with 13 integration points through the element thickness at Gaussian spacing, with an approximately square dimension of 10.2 cm (4 in.). The reinforcement is embedded in the shell elements as a uniaxial layer of steel material in each direction according to the layouts shown in Fig. 4. The hangers in Tunnel 1 are modeled using Timoshenko beam elements (B31) discretized to 7.6 cm (3 in.) with a 2.5 cm (1 in.) diameter solid circular cross-section. The hangers in Tunnel 2 utilize S4R shell elements with a length discretization of 10.2 cm (4 in.), width of 7.6 cm (3 in.), and thickness of 1.9 cm (0.75 in.). The ends of each hanger are modeled with moment continuity at their interface with the panel and at the liner anchorage. All hanger elements for both tunnels were modeled as straight and experienced sudden bifurcation when the Euler buckling load was reached due to upward blast pressure, after which they contributed zero compressive resistance. When the panel subsequently rebounds downward, the hangers will straighten and then provide tensile resistance against the dynamic reaction driven by blast-induced vibration and gravity. The shelf supports at the ends of the panels are modeled as pinned for Tunnel 1 and fixed for Tunnel 2 based on the observed fixity as previously discussed. The concrete is modeled with Abaqus' pre-programmed damage-plasticity material model (*32*), and the nonlinear shape of the plastic compressive curve and tension softening is based on the Chang-Mander concrete model (*33*). Concrete tensile strength is set equal to $7.5\sqrt{f_c'}$ per ACI 318-19 (ACI Committee 318 2019). This modeling approach has been previously validated for both one-way and two-way bending of reinforced concrete panels using published pseudo-static experimental test results (*34*, *35*).

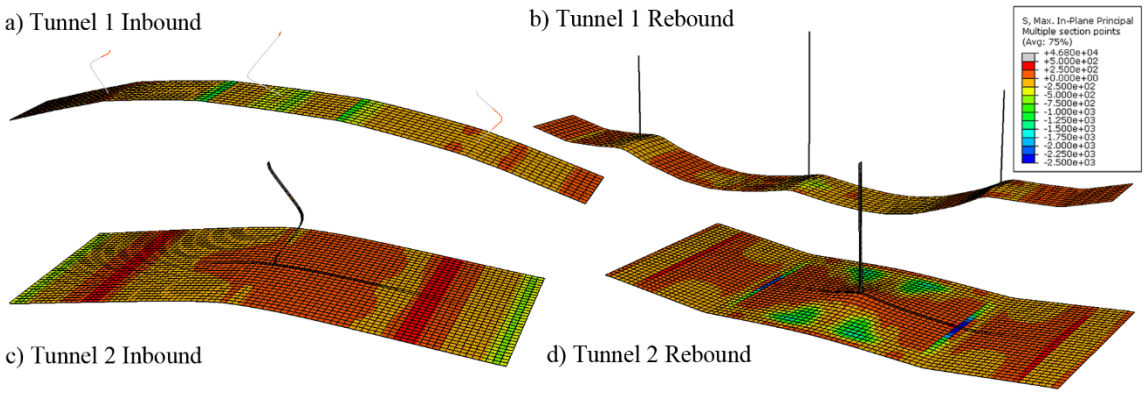

Fig. 12: Deformed shapes of FE models at maximum inbound (upward) and rebound (downward) deflection, including an overlaid contour of maximum principal stresses

Simplified right triangle blast pressure time histories, such as those shown previously in Fig. 8, are applied in the upward direction to the corresponding surface area of the ceiling panel shell elements. The displaced shapes of the FE ceiling panels at peak inbound and rebound response are illustrated in Fig. 12. During the initial upward pressure loading (i.e. inbound phase), the hangers will buckle due to a large compression reaction, after which the panel will emulate a single span in upward flexural response. On rebound, the panels will exhibit multi-span flexural response as the hangers become reengaged in tension (assuming that the integrity of the hangers or their anchorages hasn't been compromised during the inbound phase). The resistance functions obtained from FE analysis are plotted alongside those from the simplified panel spans in Fig. 11. For inbound loading in Tunnel 1, the numerical model is bounded by Cases B and D. Recall that Cases A and B assume that the hangers are not providing any resistance to upward blast loading – the numerical results show that the hangers do provide some initial stiffness during the inbound response, resulting in moderate resistance between that of the single and multi-span simplified cases. The Tunnel 1 rebound resistance of the numerical model closely matches that of boundary condition Case C as the hangers become engaged in tension. The Tunnel 2 numerical results show good agreement with the simplified resistance function for boundary condition Case IV. For the remainder of this paper, ceiling panel performance will therefore be assessed using Case IV for Tunnel 2 and a combination of Cases A and C/D for Tunnel 1.

Using the aforementioned resistance functions, the ceiling panels are simplified as equivalent single-degree-of-freedom (SDOF) models for dynamic analysis. Standard approaches have been developed to accomplish these SDOF analyses (*29*, *36*) via the development of equivalent mass and stiffness. This approach is well established for evaluating the nonlinear flexural performance of slab-like elements subjected to blast demands (*37*). The inertial mass of each ceiling panel span is assumed to be constant between the supports and equal to that of the minimum section. Damping is conservatively neglected in these analyses. Self-weight is applied as an initial condition and induces downward deflection with tension in the hangers.

The dynamic performance of the SDOF ceiling panels is quantified in terms of support rotation, which is calculated as a function of the peak deflection and span length as the panel experiences plastic flexural behavior (*29*). The peak support rotation response is assessed relative to published blast response limits for reinforced concrete elements (*38*). As summarized in Table 3, the limits used for this study correspond to reinforced concrete flexural members with no shear reinforcing

and assuming no tension membrane action. Based on these limits, the ceiling is assumed to have low damage if the maximum support rotation is less than 2°, moderate damage for 2° to 5°, high damage for 5° to 10°, and has failed if greater than 10°.

Table 3: Response limits for RC flexural members per PDC-TR 06-08 (USACE 2008)

Response Limits	μ	θ
B1	1	-
B2	-	2°
B3	-	5°
B4	-	10°

Additionally, the ceiling panels have a relatively thin section depth and low shear strength. Ceiling panels close to the explosive event will experience very high dynamic shear demands; therefore, a shear damage criterion is also included in this evaluation. The shear demand is the maximum dynamic shear computed from the dynamic shear time history, $V_R(t)$, which is computed during the SDOF analysis (*36*) in accordance with equation 1:

$$V_R(t) = C_R R(t) + C_F F(t) \qquad Eq.1$$

where $R(t)$ is the structural resistance of the equivalent SDOF system, $F(t)$ is the blast load on the system, C_R is the resistance coefficient, and C_F is the load coefficient. The load and resistance coefficients are determined based on the assumed boundary conditions, load application, and mass and stiffness distributions in accordance with standard SDOF approaches (*36*). The shear capacity is based on the lesser of direct shear capacity [$0.16 f_c' \cdot d$ per (*29*)] and shear capacity for one-way flexural response [$2\sqrt{f_c'} \cdot d$ per (ACI Committee 318 2019)], where d is the distance through panel thickness between the extreme concrete compression fiber and the tensile reinforcement. Note that the contribution of the steel reinforcement to the shear resistance is neglected. The bent reinforcement at the hanger locations in Fig. 6 resists shear due to downward gravity loading but provides insignificant shear capacity when the applied load is in upward direction.

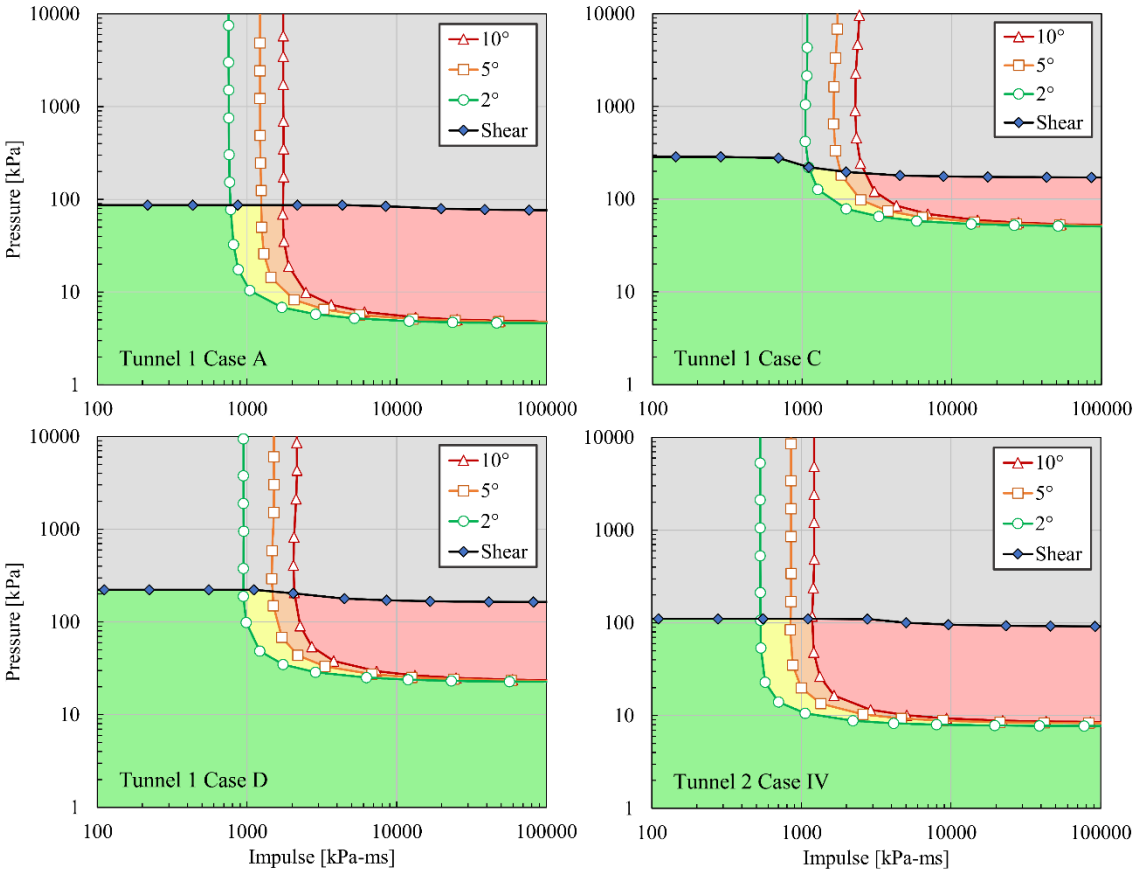

Fig. 13: Pressure-impulse iso-damage diagrams for select ceiling panel span cases

3.4 Damage Mapping

Dynamic SDOF analyses were iteratively performed for varying magnitudes of pressure and impulse to reach the flexural response limits summarized in Table 3 and shear capacity listed in Table 2. The corresponding pressure and impulse (*P-I*) iso-damage curves for each response limit are plotted in Fig. 13. The expected damage for each explosive load case is determined by overlaying the pressure-impulse demands from Fig. 9 onto the *P-I* iso-damage curves in Fig. 13. Resulting damage maps for each tunnel type and charge size are plotted over the half tunnel length in Fig. 14. The spectrum of total ceiling damage for each span condition due to each threat size in the two tunnels is summarized in Fig. 15. The results indicate that the drop ceiling will be lost over the entire tunnel length for both systems and for all boundary condition assumptions when the explosive load reaches 227 kg (500 lbs) of TNT equivalent. Due to the discontinuous top reinforcement in Tunnel 2, most of the ceiling is lost even for the smallest 22.7 kg (50 lbs) threat size. Tunnel 1 shows better overall performance than Tunnel 2 not only due to the presence of continuous reinforcement layers but also by having a larger ceiling clearance (and thus lower blast load confinement as shown previously in Fig. 9 and Table 1). The buckling resistance of the hangers plays a critical role in the response. For example, under the 45.4 kg (100 lbs) TNT charge threat the buckled hanger condition (Case A) results in 92% of the ceiling achieving heavy damage, while for the non-buckled condition (Case C/D) 0% of the ceiling reaches a heavy damage. The amount of heavy damage in Tunnel 1 reduces to less than 2% under the smaller 22.7 kg (50 lbs) TNT charge. The regions of shear failure for the 227 kg (500 lbs) charge are widespread due its

high dynamic shear demand, with approximately half of the ceiling panels reaching the shear failure limit state. Shear damage for the 22.7 kg (50 lbs) and 45.4 kg (100 lbs) charges is concentrated near the charge location – flexural damage modes will govern the response over most of the tunnel length for these threats. Overall, these results suggest that a significant amount of ceiling damage would be expected even for relatively low explosive charge sizes in both tunnels as constructed.

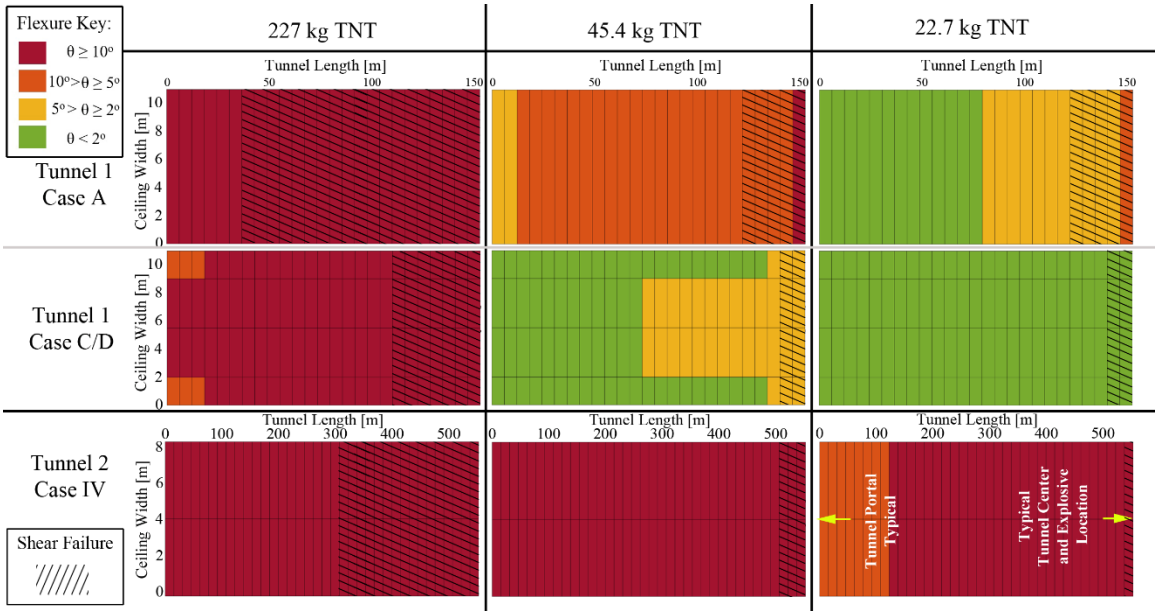

Fig. 14: Damage maps of ceiling panels for select span cases

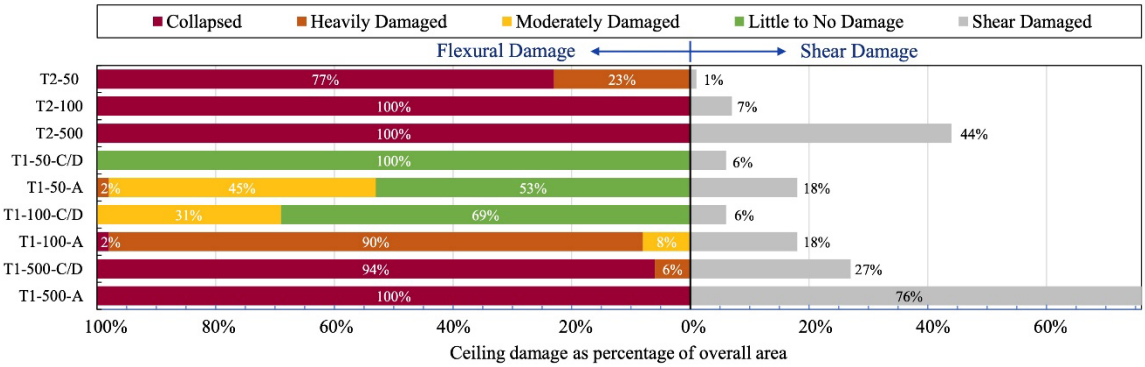

Fig. 15: Total ceiling panel damage in each tunnel for all threat sizes and span cases

3.5 Mitigation Options

To address the inherent vulnerability of these drop ceiling systems to confined blast demands, three options can be considered as potential mitigation: 1) the blast threat can be eliminated, 2) the ceiling can be removed, or 3) the ceiling can be hardened. Option 1 is not viable with current technology and traffic demands. As illustrated in Fig. 15, a relatively small blast threat can result in significant damage to the ceiling in either prototype tunnel, and detection via screening is not currently feasible. Ceiling removal (Option 2) is viable for many tunnels due to improvements in jet fan ventilation systems and modeling approaches for optimizing the locations of the fans for operational ventilation as well as smoke removal during fire events (*39*, *40*). Also, older tunnel

ceilings are often removed to reduce maintenance costs, to increase clearance (thus avoiding contact with tall trucks), and to eliminate the risk of falling panels and debris above the roadway surface due to hanger and anchorage deterioration. Hardening the ceiling (Option 3) by enhancing the flexural resistance of the panels to upward blast pressures can offer significant improvements in performance. This can be achieved by enhancing the panel flexural capacity as well as the axial capacity of the hangers. Additional hanger supports can also be added to reduce panel span lengths; however, such a retrofit would be more invasive (requiring the installation of new anchorage locations) and is therefore not considered in this study.

As shown in Fig. 14, the performance of the Tunnel 1 ceiling system is greatly enhanced when the ceiling panels act as a multi-span element (Case C/D) rather than a single span element (Case A). To consistently achieve multi-span response, the moment of inertia and cross-sectional area of the tension hangers can be increased to prevent buckling and compression failure when subjected to the inbound upward blast demands. This can be readily achieved by replacing or encasing the tension hangers with circular steel tube sections. The critical buckling load used to design the upgraded hangers can be obtained from the SDOF dynamic analyses of the tunnel ceiling with span Cases C/D, conservatively set equal to the sum of peak blast reactions from adjacent spans. The Euler buckling load for the upgraded hangers can be conservatively calculated assuming a pin-fix boundary condition with an effective length factor of 0.7. The buckling loads and reactions for each hanger (at the same locations shown previously in Fig. 3) are summarized in Table 4. To resist the inbound blast demands, an AISC Pipe 3 XX-Strong, Pipe 2½ XX-Strong, Pipe 5 XX-Strong (*41*) can be used for the middle hangers in Tunnel 1, side hangers in Tunnel 1, and all hangers in Tunnel 2, respectively.

Table 4: Properties of retrofitted ceiling hangers

Hanger Location	Tunnel 1 (Middle)	Tunnel 1 (Side)	Tunnel 2 (Middle)
Length, L	210.1 cm (82.8 in.)	139.9 cm (55.8 in.)	200.7 cm (79.0 in.)
Equivalent length, L_e	147.1 cm (57.9 in.)	99.2 cm (39.1 in.)	140.5 cm (55.3 in.)
Existing moment of inertia, I	2.0 cm^4 (0.049 $in.^4$)	2.0 cm^4 (0.049 $in.^4$)	4.4 cm^4 (0.1 $in.^4$)
Buckling load, P_{cr}	18.6 kN (4.19 kip)	41.0 kN (9.2 kip)	43.9 kN (9.8 kip)
TNT equivalent, W_{TNT}	45.4 kg (100 lbs)	45.4 kg (100 lbs)	22.7 kg (50 lbs)
Peak dynamic reaction, V_{dyn}	813.8 kN (183.0 kip)	625.6 kN (140.6 kip)	1839.9 kN (413.6 kip)
Required moment of inertia, I_{req}	89.2 cm^4 (2.144 $in.^4$)	31.2 cm^4 (0.749 $in.^4$)	184.0 cm^4 (4.422 $in.^4$)
Required cross-sectional area, A_{req}	29.5 cm^2 (4.6 $in.^2$)	22.7 cm^2 (3.5 $in.^2$)	66.7 cm^2 (10.3 $in.^2$)

Proposed retro-fit section	Pipe 3 XX-Strong	Pipe 2-1/2 XX-Strong	Pipe 5 XX-Strong
Proposed section diameter	8.89 cm (3.50 in.)	7.32 cm (2.88 in.)	14.1224 (5.56 in.)

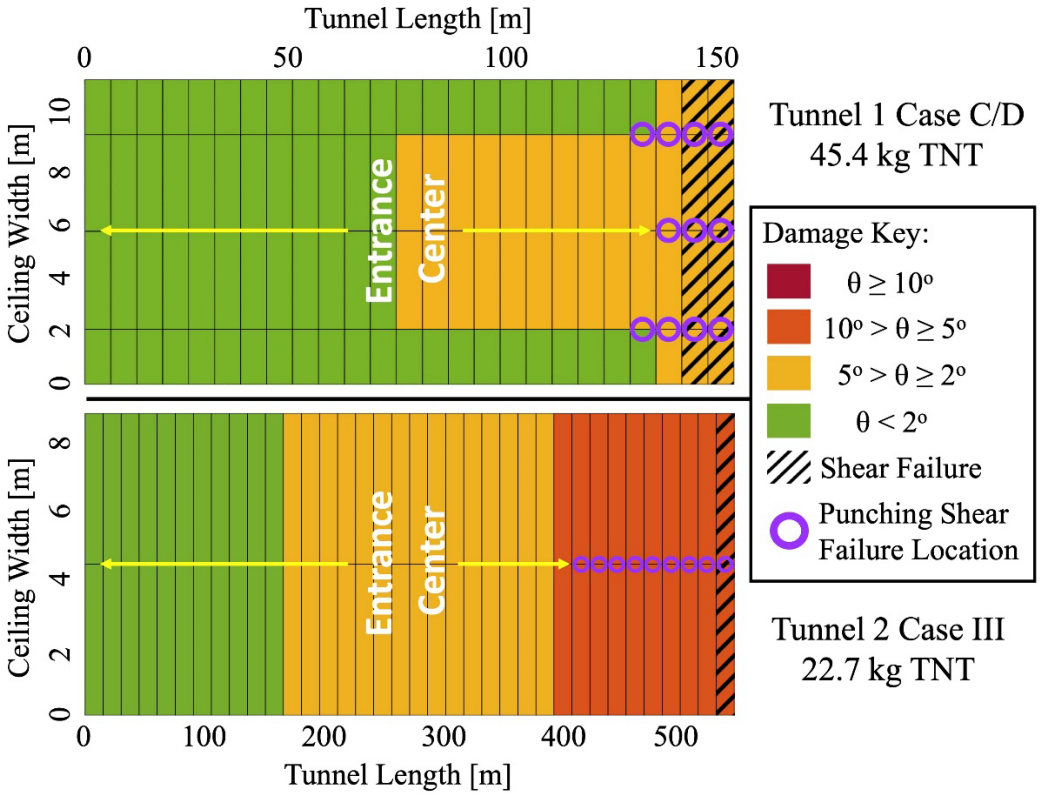

Fig. 16: Damage maps of ceiling panels with retrofitted hangers

Due to the small panel thickness, however, strengthening the hangers can result in a punching shear failure of the concrete under elevated blast demands. The dynamic shear demands determined previously by *Eq.1* are therefore compared to the punching capacity of the section in addition to the aforementioned shear limits. The concrete shear stress capacity is $4\sqrt{f_c'}$ per UFC 3-340-02 (*29*), and an equivalent square critical section of shear failure is determined with a side length of $\frac{C}{4} + d$, where C is the outside edge perimeter of the proposed retrofit pipe section. The damage maps for the in-situ ceiling panels with retrofitted hangers in Fig. 16 show that punching shear failure can extend beyond the locations of panel shear failure or heavy flexural damage. However, the overall extent of severe damage is reduced in both tunnels when the hangers are retrofitted. To mitigate punching shear failure, the panels would require local hardening at their connections to the hangers via additional reinforcement or encasement. This is increasingly important for panels that are themselves retrofitted for enhanced flexural performance, since they will impart larger reactions loads to the hangers when loaded in upward flexure.

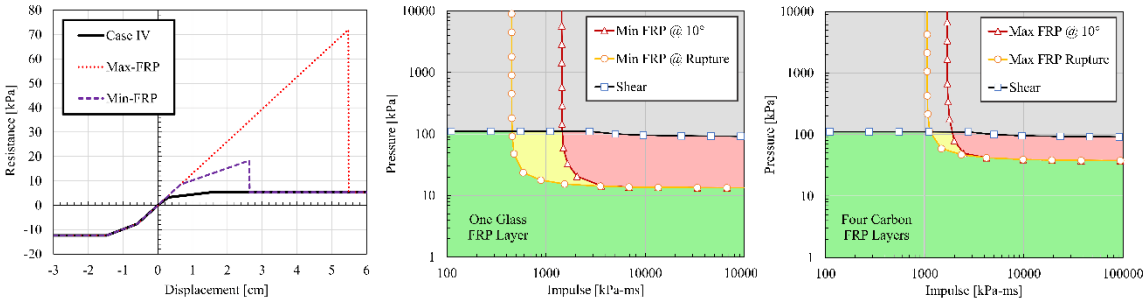

Fig. 17: FRP enhancement for Tunnel 2 ceiling panels: Case IV flexural resistance functions (left) and P-I iso-damage curves with one glass FRP layer (Min-FRP, center) and four carbon FRP layers (Max-FRP, right)

Due to its high ratio of tensile strength versus weight, fiber reinforced polymer (FRP) can be bonded to the top surface of the ceiling panels to enhance flexural resistance to upward pressure loading. FRP sheets can be installed from within the plenum space above the roadway, and their installation would only require minimal disruption to tunnel usage and operation. Unlike steel (which will undergo post-yield strain hardening), FRP provides an elastic-brittle response and will cease to contribute resistance once its capacity is reached. However, FRP retrofits that fail due to blast loading can still absorb enough energy prior to failure such that the ceiling panel experiences a lower level of flexural damage. Two levels of FRP strengthening are considered in this study: a single layer of glass FRP, and a four-layer application of carbon FRP. All FRP fibers are applied to the top face of the panel and oriented to resist one-way flexural behavior in the tunnel's transverse direction. Details of the two designs are summarized in Table 5. The resulting flexural strength is calculated in accordance with ACI 440.2R-17 (ACI Committee 440 2017). The resistance functions of the FRP retrofits were determined for Tunnel 2 as a demonstration due to its discontinuous reinforcement layout (and thus lower flexural resistance) compared to Tunnel 1. As summarized in Fig. 17, the blast resistance of the Tunnel 2 ceiling system is improved significantly with the addition of bonded FRP laminates. Even in the case with the single FRP layer, enough energy is absorbed before the FRP fails to mitigate most instances of structural failure (at support rotations past 10°).

Table 5: Details of FRP Retrofit Solutions

FRP Solution	Max-FRP	Min-FRP
Material	Carbon FRP	Glass FRP
No. of Plies	4	1
Thickness	0.13 cm (0.05 in.)	0.81 cm (0.32 in.)
Area per ft.	3.48 cm^2 (0.54 $in.^2$)	22.32 cm^2 (3.46 $in.^2$)
Ultimate Strength	883 MPa (128 ksi)	386 MPa (56 ksi)
Elastic Modulus	98 GPa (14200 ksi)	23 GPa (3300 ksi)

The improvement in performance is evaluated with respect to three response levels: structural failure (support rotation exceeds 10°), FRP failure (when stress in the FRP laminate reaches its ultimate strength but the support rotation of the panel does not exceed 10°), and low damage (with

support rotation less than 2°, which keeps the FRP laminate in its elastic range). The resulting damage map for the FRP retrofitted panels in Tunnel 2 is shown in Fig. 18 for the 22.7 kg (50 lbs) and 45.4 kg (100 lbs) charge sizes. The minimum FRP retrofit is able to prevent panel failure for the lower 22.7 kg (50 lbs) hazard (with the majority of the ceiling experiencing moderate damage and FRP failure) but is unable to provide any tangible benefit against larger threats as the entire ceiling still fails for the 45.4 kg (100 lbs) threat. The maximum FRP option provides significant damage reduction against the lower hazard (with only 8.3% of panels experiencing moderate damage and none failing), though 25% of the ceiling area still collapsed when subjected to the larger hazard. Further flexural enhancement could be achieved in theory by applying additional layers of FRP, but increased layering could eventually be impractical due to limitations on the bond interface to achieve composite behavior.

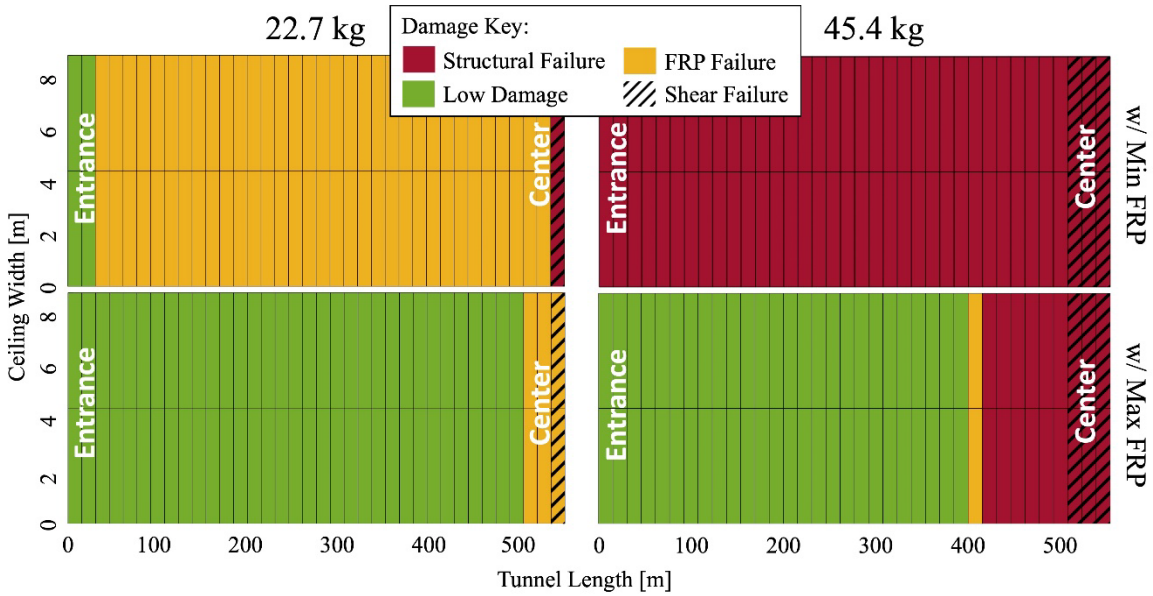

Fig. 18: Damage maps of FRP-retrofitted Tunnel 2 ceiling panels (Case IV with upgraded hangers)

The choice of mitigation strategies will be influenced not only by performance objectives and/or risk tolerances but also by operational requirements and cost. Many existing tunnel ventilation systems are reliant on the presence of the drop ceiling to create the plenum above the roadway. Replacement of these systems would be an additional cost beyond removal of the ceiling panels, and the application of FRP to the top surface of the panels would enable the preservation and continued operation of those systems. However, as shown in Fig. 18, the FRP retrofit options may only provide enhanced resistance against lower level blast threats with little to no benefit against larger threat sizes that could damage the tunnel liner itself (i.e. 227 kg (500 lbs) and higher per Bai et al. [2018]). Based on conversations with several industrial contacts, the approximate estimated costs of material and installation for the minimum (single-ply glass) and maximum (quadruple-ply carbon) FRP mitigations are \$160/m^2 (\$15/ft^2) and \$1075/m^2 (\$100/ft^2), respectively. The estimated costs of the two FRP options for Tunnel 1 based on the total area of ceiling panel is approximately \$530,000 and \$3.5 million; likewise, the estimated costs for Tunnel 2 are \$1.6 million and \$10.2 million, respectively. Note that these cost estimates do not include the additional cost of hanger upgrades, which would be needed to resist the reactions from the FRP-enhanced spans. Installation of FRP and upgraded hangers could potentially be accomplished with only

minimal operational impact since almost all construction activities would occur in the plenum space above the roadway.

Removal of the drop ceiling would be significantly more impactful to the tunnel's operation, most likely requiring periodic closures at night or on weekends over a period of 2-4 years. Also, the ventilation system would need to be replaced or upgraded with jet fans when the plenum is eliminated. However, removing the ceiling panels not only eliminates their collapse potential during a blast event but also reduces the confinement of the explosion, which can alleviate the resulting pressure and impulse imposed on the tunnel structure. Based on the recent removal of drop ceilings in two Pennsylvania tunnels (*4*, *43*), the cost of demolition and removal is estimated to be \$775/m^2 (\$72/ft^2), not including the installation of new ventilation systems. Based on this figure, the estimated cost of drop ceiling removal would therefore be \$2.6 million for Tunnel 1 and \$7.4 million for Tunnel 2. Based on data published by the Colorado Department of Transportation (*44*), the estimated cost of jet fan installation (including power supply and conduit) for the Eisenhower-Johnson Memorial Tunnel (2 lanes per bore over a length of 2.72 km) ranged from \$10 million to \$16 million depending on the ventilation objectives per traffic volume as well as smoke management for an enclosed fire. Even though the added cost of fan installation would factor into the decision to remove rather than retrofit the ceiling panels, jet fans can potentially offer lower long-term operating and maintenance costs with greater air movement efficiency compared to legacy systems which rely on the plenum above the roadway.

Chapter 4: Case Study of Tunnel Drop Ceilings Exposed to Fire

The results of drop ceilings assessment when subjected to explosions illustrate the vulnerability of this tunnel component under blast events. A more common threat scenario in transportation tunnels is accidental fire events. The susceptibility of the ceiling panels to fire induced failure is examined in two representative tunnels using standard fire curves as well as several realistic fires due to vehicular accidents. Standard fire demands per the RWS and ASTM E1529 fire curves are uniformly applied to the ceiling panels, while the heat exposure contours for typical vehicle fires with heat release rates of 30 MW, 100 MW, and 200 MW are generated from the software CFAST. The finite element analysis software SAFIR is used to evaluate the thermo-mechanical behavior of the ceiling panels when subjected to various thermal demands from the fire below.

4.1 Fire Characterization

Fire-induced thermal demand on the drop ceiling panels can be represented using either standard fire curves or a parametric fire model. Standard fire curves are commonly used to develop fire resistance ratings for both structural and non-structural components. These prescribed temperature time histories include a fast ramp-up to a high temperature, which is then maintained until a failure criterion is reached at a time that signifies the fire resistance. The Rijkswaterstaat (RWS) standard time-temperature curve (see Fig. 19) is commonly used to develop fire resistance ratings for tunnel structures and components. The RWS curve is based on experimental results for a 50-m^3 fuel tanker truck fire with a heat release rate (HRR) of 300 MW and a 2-hr duration (*45*). The current standard of practice according to NFPA 502 (*11*) states that tunnel structures should be capable of resisting the full 2-hr duration of the RWS or another recognized standard fire curve that is acceptable to the authority having jurisdiction. Since the time history of the RWS curve is tailored to this 2-hr fire resistance requirement, analyses using the RWS curve in this study will immediately drop the compartment temperature to ambient (20°C) after the 2-hr milestone. This "shutdown" of the RWS curve is used to allow a component that has survived the 2-hr exposure (thus meeting the NFPA 502 fire resistance requirement) to then undergo subsequent cooling. A similar approach to implementing the RWS curve was used by the authors to evaluate the residual state of the tunnel liner for a range of fire sizes (*15*).

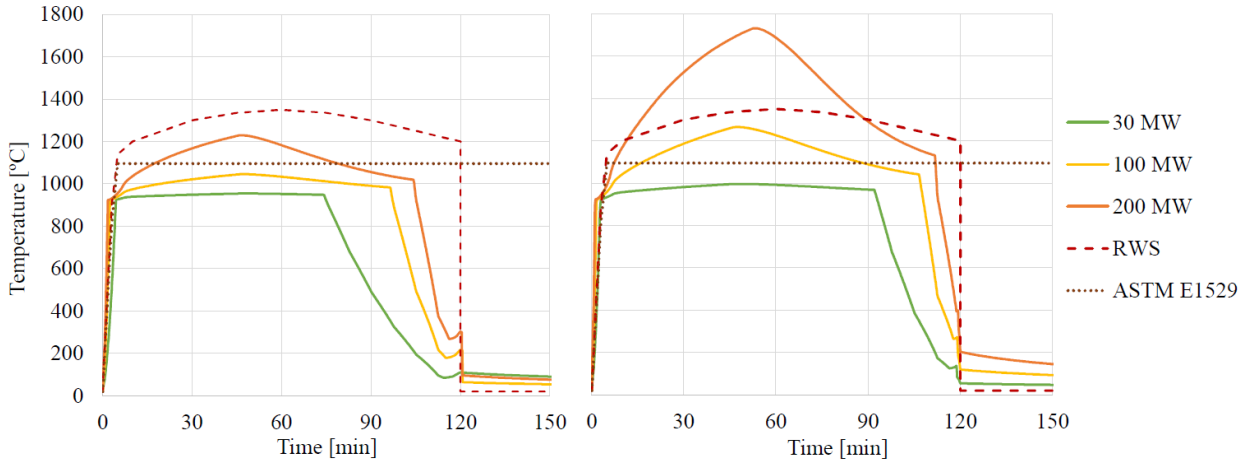

Fig. 19: Temperature time histories at the transverse and longitudinal center of Tunnel 1 (left) and Tunnel 2 (right)

Also plotted in Fig. 19 is the ASTM E1529 standard curve (*46*), which represents exposure to a large hydrocarbon fire by prescribing a rapid increase to 1095°C in 5 min followed by an indefinite period of constant exposure at that temperature until the failure criteria is reached. The thermal demands from standard fire curves are typically applied uniformly over the entire exposed surface of a component. The implementation of these curves is generally expected to represent an upper bound.

Though useful for characterizing fire resistance, standard fire curves do not represent the spatial distribution and time history (which includes a ramp-up to peak exposure followed by decay toward burnout) that are typical of a realistic localized fire. Fire growth and smoke transport modeling using numerical tools such as CFAST (*47*) can be used as a performance-based alternative to standard fire curves to determine the spatial and temporal thermal demands on structural and architectural systems as a result of a particular fire hazard. The CFAST approach, predicated on the framework described in ASTM E1355 (*48*), is based on a two-zone fire model that is capable of simulating the environment in a single- or multi-compartment structure subjected to fire. The software calculates the time-evolving distribution of smoke and gaseous combustion products as well as the temperature throughout a user-defined compartment during a user-prescribed fire (*49*). The fire drives combustion products from the lower to the upper layer via the plume, and the temperature within each layer (which are assumed to be "well-mixed") is approximated as uniform. The transport of smoke and heat between zones is dictated by empirical correlations (*50*). Though more complex to implement than standard fire curves, zone models require significantly less effort than numerical solutions predicated on computational fluid dynamics (*51*, *52*).

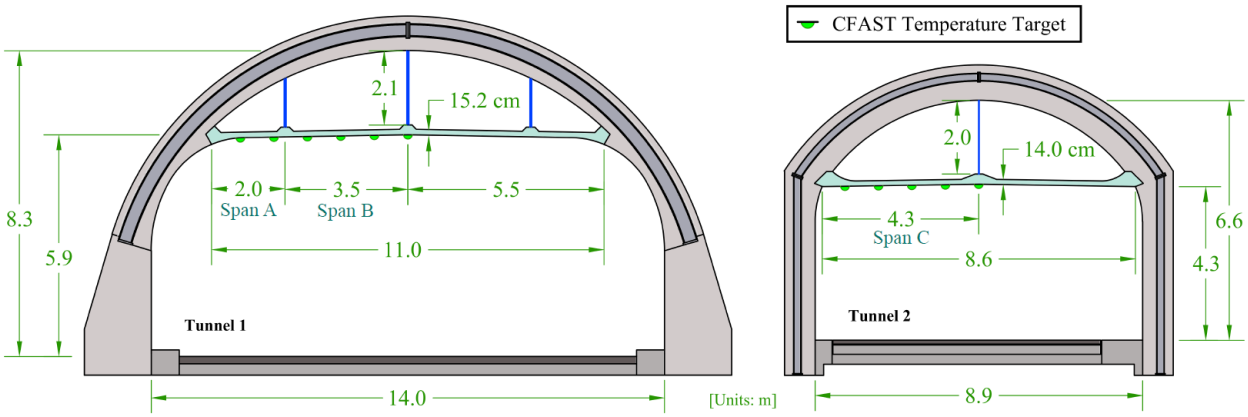

Fig. 20: Prototype tunnel cross-sections and CFAST Temperature Target Locations

As shown in Fig. 20, a series of temperature gauges are placed at 31.4-cm (3-ft) intervals under the ceiling panel along the longitudinal and transverse direction to record the temperature time history during the 30 MW, 100 MW and 200 MW fire scenarios. CFAST models of these localized fires in both prototype tunnels assume a fire location at the longitudinal and transverse center of the tunnel. Initial conditions in the compartment are at 20ºC with standard atmospheric pressure and 50% humidity in air. The compartment is defined as a cuboid with user-defined cross-sectional area versus height and an opening at each end to the ambient environment. For each scenario, the HRR time history includes an initial quadratic ramp-up, a constant steady-state stage, and then an exponential decay according to Ingason et al. (*53*). CFAST then calculates the temperature exposure at each gauge due to the combustion at the fire location. Specifically,

CFAST computes the fire-induced thermal demand based on the fuel's chemical formula and heat of combustion, combined with the oxygen content following the fundamental laws of mass and energy conservation. A vehicle fire realistically includes an eclectic combination of solid and liquid fuels; an HRR-equivalent hydrocarbon pool fire (which is much easier to simulate using published data and semi-empirical models) was therefore utilized similar to a previously published study by the authors (*16*). The vehicle fire is approximated with a gasoline (C_8H_{18}) pool that is elevated two feet from the roadway surface to approximate a generic bumper height. The heat of combustion of gasoline is taken as 43,700 kJ/kg (*54*).

The current version of CFAST has a 100-m length limitation on any single dimension of the compartment. Since the length of both tunnels exceeds this limit, a sensitivity study was initially performed to determine the impact of the compartment length on the predicted temperatures. The cross-sections of both tunnels were modeled in CFAST with lengths ranging from 60 to 100 m, and the longitudinal ends of the compartments were defined as "open" (beyond which ambient temperature and pressure conditions are assumed). While most drop ceiling panels have ventilation openings, these openings were neglected in this study, and no forced ventilation is applied in the CFAST compartment model below the drop ceilings for additional simplification. These assumptions ensure an upper-bound buildup of hot gases and smoke within the tunnel below the drop ceiling. In some cases, forced ventilation can "stoke" an enclosed fire and slightly increase the HRR of the burning fuel via increased oxygen supply (*55*, *56*). This effect could be considered in subsequent phases of this research, but the current study simplifies each fire scenario as having a constant HRR.

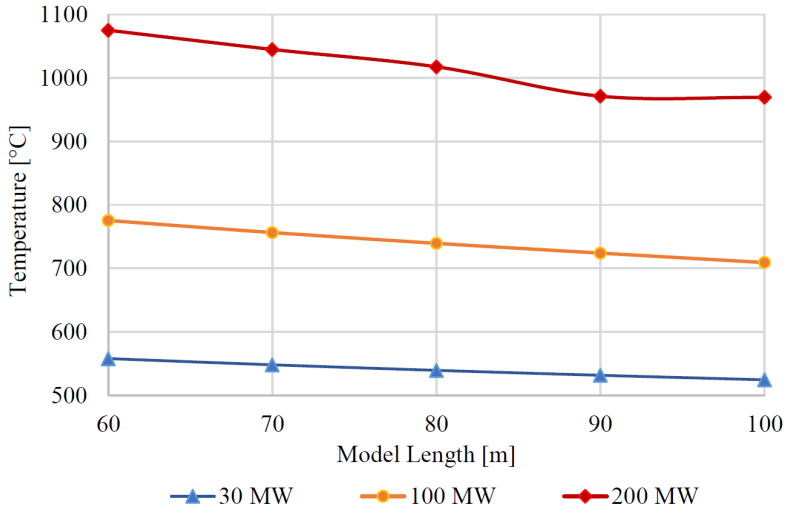

Fig. 21: Maximum temperature at the transverse end of the drop ceiling at the longitudinal center of the tunnel with varying CFAST compartment length

Fig. 21 shows only a 5-10% reduction in maximum temperature as the length of the compartment increases from 60 m to 100 m. Shorter compartments will experience a slightly greater artificial buildup of combustion byproduct before it exits through the open boundaries, which also provide more fresh oxygen to stoke the combustion reaction when at closer proximity to the fire. Based on the slope of the lines plotted in Fig. 21, the maximum temperature would undoubtedly decrease further with increased compartment length. The 100-m long compartment is therefore conservatively adequate for the evaluations performed in this study.

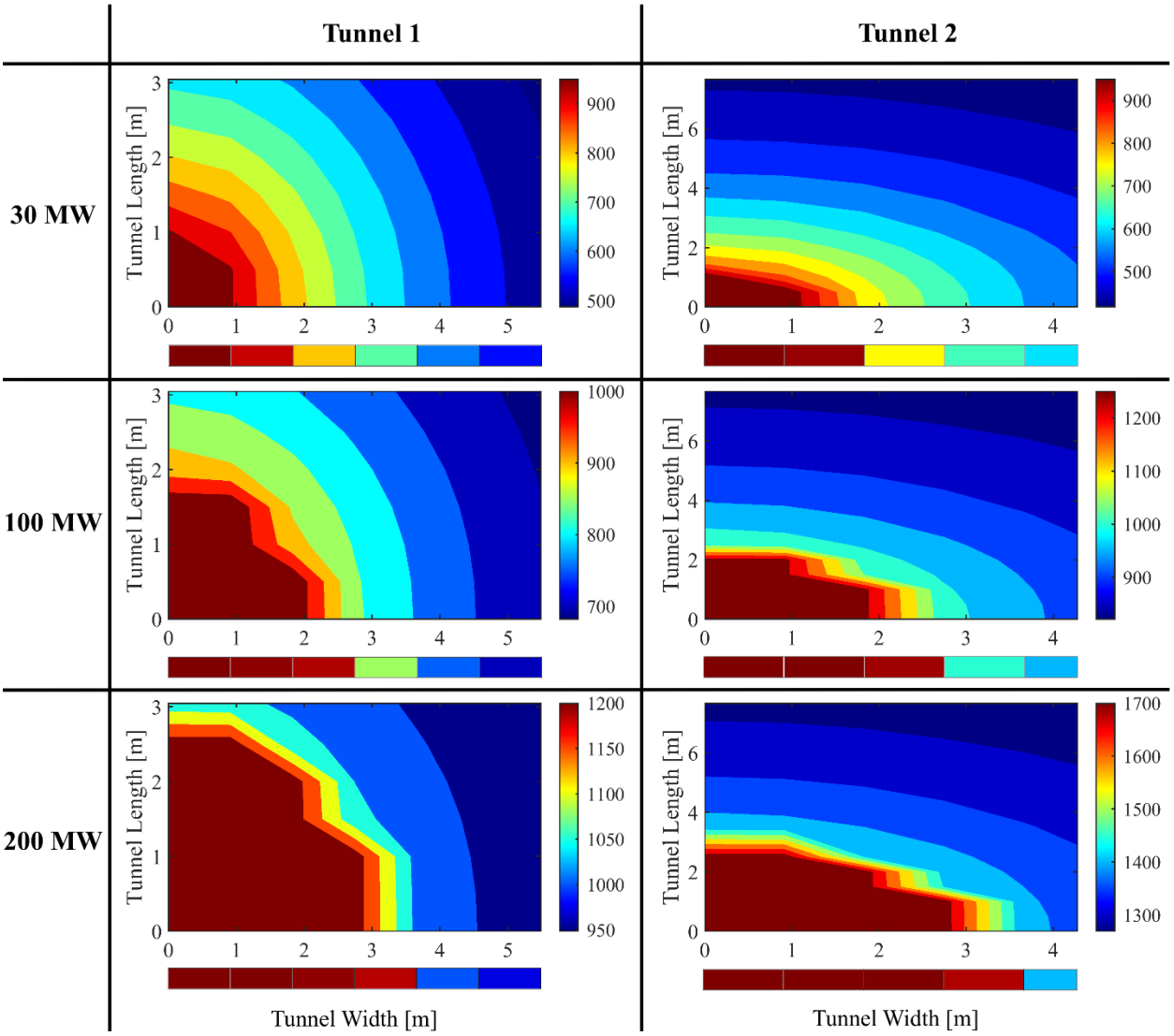

Fig. 22: Symmetric contours of peak temperature distribution (with the origin directly over the fire)

Fig. 19 includes the plotted temperature time histories for the 30 MW, 100 MW, and 200 MW fire scenarios at the longitudinal and transverse center of each tunnel using the 100-m CFAST compartment length. Fig. 22 shows the contour of maximum recorded temperature which emanates from the fire location. Due to its smaller cross-section and lower ceiling height, Tunnel 2 experiences higher overall temperature due to the increased confinement of the fire than Tunnel 1. The peak temperatures are generally comparable to those shown for the RWS and ASTM E1529 standard fire curves. The exception is the 200 MW case in the smaller Tunnel 2, which confines the large amount of combustion products to develop a peak temperature just greater than 1700°C. These temperatures are approximately 25% higher than the peak temperatures recorded during fire tests in the Runehamar tunnel (whose cross-section has similar dimensions as Tunnel 2) in Norway for a 200 MW fire (*57*). It is important to note that the Runehamar 200 MW fire test included forced ventilation at critical velocity, which it commonly implemented to mitigate the effects of

fire in tunnels (*58*) and can decrease the maximum recorded temperature due to increased longitudinal air flow (*59*).

4.2 Thermo-Mechanical Analysis Approach

This study focuses on the thermo-mechanical performance of the drop ceiling panel right above the fire location, which experiences the highest temperature in the absence of forced ventilation and is therefore most likely to fail when subjected to localized fire. Thermo-mechanical analysis of the ceiling panels are conducted using the specialized finite element software SAFIR, version 2016c.0 (*60*). A transverse strip of the ceiling panel is modeled with a width based on the reinforcement spacing in that direction (121.9 cm for Tunnel 1 and 25.4 cm for Tunnel 2). The thickness used in the analyses of each panel is based on the minimum thickness shown previously in Fig. 20. By applying the time history of heat exposure to the bottom surface of the ceiling panel, SAFIR can calculate the time-dependent temperature gradient through the thickness of the panel and the resulting structural response, which includes material weakening and thermal expansion. Although the exhaust smoke and gas can heat the top surface of some panels near the fire location, that heat transfer will be mitigated significantly via turbulent mixing with the cooler supply air. The top surface of the panel is therefore simplified as having ambient exposure for the thermal analyses in this study.

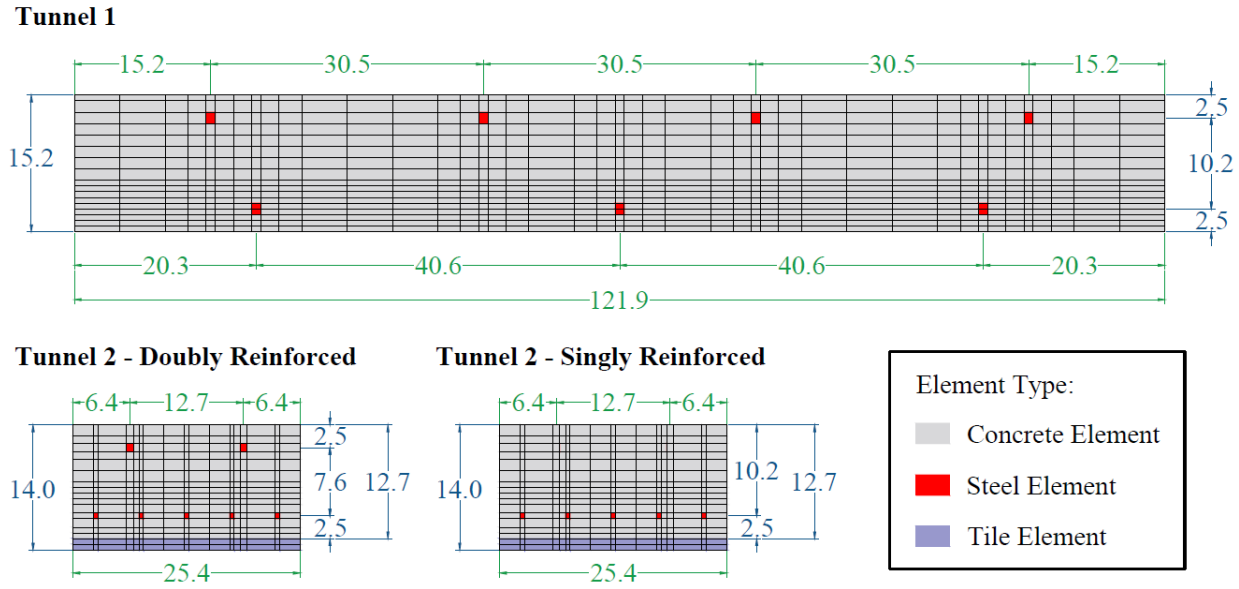

Fig. 23: Fiber layout in the panel cross-sections (units in cm)

The meshed layout of each panel cross-section is shown in Fig. 23. The red fibers represent the location of steel reinforcing bars, which have the same area as the actual circular bars. The low thermal conductivity and high specific heat capacity of concrete result in a large temperature gradient between the exposed and unexposed surfaces, and the mesh near thermal frontier is therefore finer. The concrete material is defined as calcareous with thermal conductivity and specific heat at room temperature assumed to be 2.0 W/m-K and 900 J/kg-K. These values are temperature dependent per the constitutive model for normal weight concrete in Eurocode 2, Part 1-2 (*61*), with the variation in thermal conductivity taken as the average of the upper and lower

bound. Thermal properties for the steel reinforcement are also taken according to Eurocode 2 (*61*). As shown in Fig. 23, the bottom surface of the Tunnel 2 drop ceiling is tiled. The 1.3-cm thick layer of tile and grout are assumed to have constant thermal properties with a thermal conductivity of 1.1 W/m-K, a specific heat capacity of 850 J/kg-K, a density of 2310 kg/m^3, and zero water content per a published study of thermal properties for common ceramic tiles (*62*).

The surface emissivity of the concrete and tile are taken as 0.80 (*61*) and 0.95 (*62*), respectively. The convective heat transfer coefficient on the fire-exposed surface is taken as 50 W/m^2-K per the recommendation of Eurocode 1, Part 1-2 for a hydrocarbon fire (*63*). However, the Eurocode does not specify the convective heat transfer coefficient on the unexposed side of members when forced ventilation is considered. The *Guidelines for Emergency Ventilation Smoke Control in Roadway Tunnels* (*64*) specifies a minimum airflow velocity of 11.0 m/s in order to maintain acceptable air quality levels at the tunnel's exit portal. Recent experimental studies have reported convective heat transfer coefficients from 19 to 26 W/m^2-K for the top faces of concrete blocks that are subjected to air flow velocities ranging from 3.5 to 10 m/s (*65*, *66*). Based on those studies, the convective coefficient on the top face of the drop ceiling panels (which is assigned a constant ambient temperature of 20°C) is conservatively approximated as 25 W/m^2-K for this study. The vertical surfaces of the panel cross-section are modeled as adiabatic per the simplifying assumption of uniform exposure over the width of the panel.

Heat transfer to the tension hangers in Fig. 20 is neglected since they will be shielded from fire exposure by the ceiling panels and exposed to the ventilating airflow (which is moving at relatively high velocity and turbulently mixes with the cooler supply air in the plenum). Heat transfer to the hanger anchorages is also neglected for this study since the temperature of the unexposed face of the ceiling panel will remain relatively low (i.e., below 150°C) during fire exposure. However, the sensitivity of these connections to lower magnitudes of temperature increase is recommended for future study since little data is available in the current literature.

Thermal analysis in SAFIR is performed by applying a fire temperature time history to the bottom face of the discretized cross-section and then obtaining the temperature time history in each fiber. These results are then used as thermal input for dynamic structural analysis in the 2D vertical plane. Due to the relatively slow onset of fire-induced response relative to seismic or blast loading, zero damping is conservatively assumed. The panels are analyzed using 3-noded fiber-beam elements, which are discretized to a maximum 15.2-cm (6-in.) element length (*67*) with the same cross-section mesh shown in Fig. 23. For standard fire cases, the prescribed temperature time history is applied uniformly over the span of the ceiling panel in the tunnel's transverse direction. For the CFAST cases, the temperature application is mapped along the panel span using the contours shown in Fig. 22. Specifically, the recorded CFAST temperature time histories are applied as equally spaced zones (12 zones for Tunnel 1 and 10 zones for Tunnel 2) to the discretized fiber-beam elements across the panel span per the contour bars shown below each plan map.

To represent their interface with the shelf supports shown in Fig. 20, the transverse ends of the ceiling panels are modeled as rotationally pinned for Tunnel 1 and fixed for Tunnel 2, similar to a previous study by the authors regarding the blast resistance of these structures (*13*). Horizontal and vertical translation is fully restrained at all panel ends. The tension hangers in Fig. 20 are modeled as spring elements with constant stiffness equal to EA/L (E = elastic modulus, A = hanger cross-sectional area, L = length of hanger). An asymmetric axial elastic-perfectly-plastic constitutive

model is used for the hanger springs. The limiting compression and tension forces are set equal to the ambient buckling load and tensile capacity, respectively, for the hangers in each tunnel.

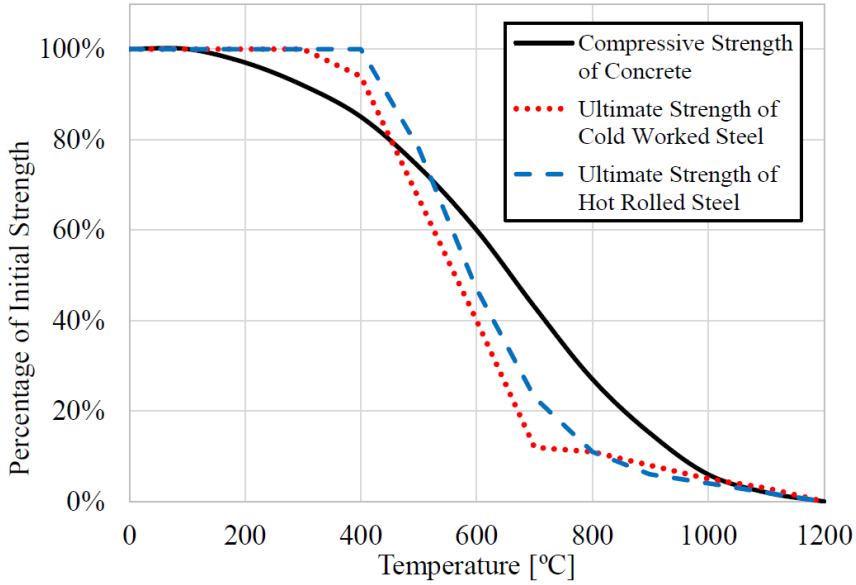

Fig. 24: Temperature-dependent reduction of compressive strength for calcareous normal weight concrete and ultimate strength of cold-worked and hot-rolled steel (*61*)

Gravity loading corresponding to the self-weight of the panel is uniformly applied as a constant line load along the panel span per the extreme load combination in ASCE 7-16 (*68*) (assuming no live load). Concrete and steel are modeled with temperature dependent reduction factors per Eurocode 2, Part 1-2 (see Fig. 24) (*61*). Steel structural properties are assumed to be fully recoverable after cooling (*69*). Permanent residual reduction of concrete strength is based on Eurocode 4, Part 1-2 (*70*) as an additional 10% below the maximum reduction experienced in each concrete fiber during heating. The tiles are assumed to contribute negligible structural resistance and are therefore neglected in the structural analysis. Based on the age of the systems and their design drawings, the steel reinforcement was assumed to have a yield strength of 276 MPa (40 ksi) for hot-rolled steel bars and cold-worked welded wire mesh (*18*). The compressive strength of the concrete is conservatively estimated to be 20.7 MPa (3000 psi) with tensile strength equal to 13.7% of compressive strength (2.8 MPa). The stress-strain model for calcareous concrete includes explicit transient creep (*71*), which promotes an increasingly accurate prediction of residual deflections in fire-exposed reinforced concrete elements per recent research by the SAFIR developers (*72*, *73*). Tensile cracking is modeled using a smeared crack model with a descending branch to zero stress. Crack closure is modeled using a stress-strain path directly back to the origin, at which point compressive stress-strain behavior can resume.

4.3 Fire-Induced Damage

The fire resistance of these ceiling panel systems is assessed in terms of failure time from the results of thermo-mechanical analysis in SAFIR. For a standard fire test of structural components in flexure, ASTM Standard E119 (*74*) outlines a 2-step definition of "failure": once maximum deflection exceeds $L^2/400d$, then the maximum deflection rate must exceed $L^2/9000d$ per minute as determined over 1 minute intervals (L = clear span of the beam, d = distance between extreme fibers of tension and compression). For this study, the maximum deflection criteria are typically

not reached during the analyses since the thin ceiling panels deflect very rapidly when approaching "failure," at which point the structural analysis no longer converges as the element approaches runaway deflection (thus exceeding the maximum deflection rate). The onset of runaway deflection is therefore used as the failure criteria.

Table 6 Summary of Ceiling Panel Failure Times for Various Fire Scenarios

Tunnel	Span	Length (m)	Critical Deflection Rate (cm/min)	Failure Time (min)				
				E1529	RWS	200 MW	100 MW	30 MW
Tunnel 1	A	2.0	0.3	214	164	328	312	344
	B	3.5	1.0					
Tunnel 2	C	4.3	2.0	90	74	75	108	316

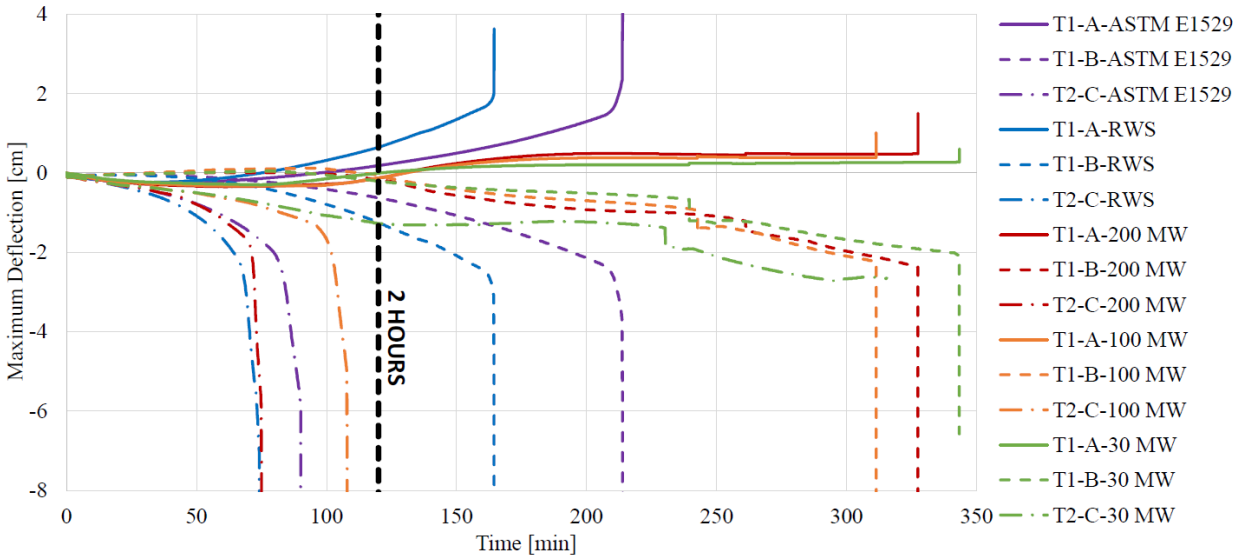

Fig. 25: Vertical deflection time histories at the critical points for all fire scenarios in (a) Tunnel 1 (T1) and (b) Tunnel 2 (T2)

The failure times obtained from all thermo-mechanical analyses are summarized in Table 6, and time histories of vertical deflection at the critical points along the each panel span are plotted in Fig. 25. Almost all analyses exhibit a rapid increase in deflection and cease to converge within a few minutes of exceeding the ASTM E119 maximum deflection rate. Representative failure modes of the two drop ceiling panels in Fig. 26 show that both exceed the deflection rate criteria due to plastic hinge formation. The Tunnel 1 ceiling panel first hinges near the midspan of Span B in Fig. 20due to positive bending moment, followed by the development of a second hinge in Span A due to the subsequent accumulation of negative moment. The Tunnel 2 panel first hinges due to negative bending at the location where the top reinforcement terminates. The panel then

approaches runaway vertical displacement in the adjacent span due to subsequent accumulation of positive bending.

Fig. 25 clearly shows the time at which the deflection accelerates toward failure with the exception of case T2-C-30 MW. In that case, the structural analysis experienced sudden non-convergence due to the loss of load carrying capacity and was unable to achieve any subsequent deflection toward runaway.

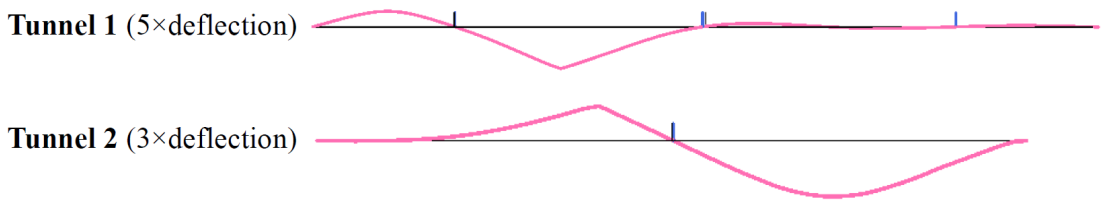

Fig. 26: Representative shapes of the drop ceiling fiber-beam element models at the time of failure

The Tunnel 1 panel achieves more than double the fire resistance rating for the E1529 standard fire exposure as the Tunnel 2 panel, primarily due of the presence of continuous flexural reinforcement and shorter spans between hanger supports. When the panel is actively heated, its materials will undergo thermal expansion (which is restricted by the boundary conditions and induces additional reactions) as well as a decrease in strength and stiffness. The panels develop a significant thermal gradient through their depth due to concrete's low thermal diffusivity, and the restraint of thermal expansion (particularly in the hotter fire-exposed bottom face) will therefore induce both compression and additional negative bending moment along the panel span. The combination of material weakening with the increase in restraining stress eventually leads to a plastic mechanism and runaway vertical deflection under self-weight.

For the RWS exposure, the Tunnel 1 panel again achieves more than twice the time to failure as the Tunnel 2 panel. However, it is important to note that the Tunnel 2 panel fails during the 2-hr fire duration (with a similar mode as for the E1529 exposure) and the Tunnel 1 panel fails during the cooling phase (after the RWS fire has been "turned off" as shown previously in Fig. 19). If a panel is able to withstand the material weakening and increased restraining forces to reach the end of active heating, then it will begin to cool and contract as thermal expansion attenuates. The panel will typically experience permanent deflection and shortening due to the combination of material weakening and restraint of thermal expansion during the heating phase. As the panel cross-section cools, fibers that have permanently shortened will begin to experience tension, leading to concrete cracking, significant reductions of residual moment capacity, and the development of post-fire plastic mechanisms that can lead to runaway deflection. The Tunnel 1 panel experiences this type of failure nearly 45 minutes after the shutdown of the RWS fire, though its shape at failure is nearly the same as that shown in Fig. 26.

The Tunnel 1 panel experiences a similar failure during the cooling phase for exposure to all CFAST scenarios, with the time to failure decreasing as the peak HRR increases. Note that the time to failure for all CFAST cases is almost double that for the RWS case since the panel span is subjected to spatially varying heating per Fig. 22 (with fire temperatures tapering toward the ends of the span) rather than uniform heating per the RWS scenario. The Tunnel 2 panel only reaches the cooling phase for the 30 MW scenario and experiences a similar failure during the cooling phase as the Tunnel 1 CFAST cases. The Tunnel 2 panel is unable to survive the active heating

duration of the 100 and 200 MW scenarios or the 2-hr RWS duration before experiencing runaway deflection.

These results highlight the importance of considering the cooling period when evaluating the resistance of tunnel components to realistic fires. The duration and maximum intensity of those fires will determine the response of a panel that survives the active heating phase. The structural response to a continuously applied standard fire curve like the E1529 can provide a relative measure of fire resistance between various component types and designs, but such evaluations do not necessarily describe the ability of the component to survive a realistic fire event to burnout. Rather, a component's E1529 fire rating could be correlated to its ability to survive one or more realistic fire events. For example, the 1.5-hr E1529 rating for the Tunnel 2 panels correlates to structural failure during heating in most other scenarios. The 3.5-hr E1529 rating for the Tunnel 1 panels indicates that these components are able to survive the 2-hr active heating duration of all other scenarios but then fail during cooling. An even greater E1529 rating could potentially indicate that a panel could survive a realistic fire scenario through the cooling phase, after which its post-fire residual damage could be assessed. In that case, the amount of post-fire damage could be used to evaluate fire resilience (i.e., the loss of functionality and the resources needed for repair or replacement).

All cases illustrated above assume that the cross-sections shown in Fig. 23 are intact throughout the analysis of the panel; however, fire-exposed concrete and tile can spall when subjected to the severe thermal demands of a tunnel fire (*75–78*). The sudden loss of concrete, tile, or other coverings during the fire due to severe cracking, differential thermal expansion, or explosive spalling will reduce the cover and increase the temperature in both the steel reinforcement and the remaining concrete section. Over the past several decades, numerous experimental studies have examined the spall potential of fire-exposed concrete, but a consensus on a predictive model has not been reached. Recent testing has indicated that spalling typically occurs within the first 10 minutes of exposure to severe fires (similar in peak temperature and ramp-up to those considered in this study) and can penetrate to a depth ranging from 1-3 cm (0.4-1.2 in) (*79*).

Table 7 Summary of Spalled Ceiling Failure Times for Standard Fire Exposures

Tunnel	Spall Scenario	Span	Length (m)	Critical Deflection Rate (cm/min)	Failure Time (min)	
					E1529	RWS
Tunnel 1	Concrete	A	2.0	0.3	113	91
		B	3.5	1.0		
Tunnel 2	Tiles	C	4.3	2.0	70	60
	Concrete and Tiles				36	31

To demonstrate the deleterious impact of fire-induced spalling, the standard fire analyses of the two ceiling panels are repeated with a thin layer of concrete and/or tile removed to represent spalling. For the Tunnel 1 panels, 1.75 cm (0.69 in.) of concrete is removed from the fire-exposed face. For the Tunnel 2 panels, two scenarios are considered: with only the tile layer removed, and with both the tile and 1.75 cm of concrete removed. Rather than attempting to estimate the time or

location of spalling, the material removals are conservatively applied over the entire span of the panels at the onset of the fire. As shown in

Table 7, the failure times for the drop ceiling panels with 1.75 cm of spalled concrete are approximately halved compared with those of non-spalled cases in Table 6. The Tunnel 2 cases with only the tiles removed experience a 17-20% reduction in failure time due to a faster transmission of heat into the structural concrete section. Failure modes for the spalled cases are again similar to those shown previously in Fig. 26. All RWS cases now fail during the 2-hr active heating period. These results highlight the potential impact of spalling on the performance of these thin reinforced concrete systems. In practice, a stochastic approach based on the experimental literature could be used to develop a more holistic estimation of fire resistance.

Chapter 5: Summary and Conclusions

This study assessed the performance of drop ceiling systems in two prototype tunnels when subjected to blast loading and temperature demands from standard and natural fires on the roadway below. The ceilings are composed of thin reinforced concrete panels that span primarily one-way in the transverse direction and are supported by the tunnel liner via ledge supports and tension hangers.

For the evaluation of drop ceiling under blast demands, the expected impulsive pressure demands due to the detonation of design-basis explosive threats per published guidelines were determined via computational fluid dynamic analysis using the commercially available software package ProSAir. The flexural and shear resistance were determined using idealized mechanical models and verified against finite element (FE) analyses in Abaqus. Dynamic SDOF analyses with these resistance functions were used to assess the potential for blast-induced damage to the existing ceiling panels as well as the improvement offered by two FRP retrofit options. The choice of between retrofit or removal of the drop ceiling to mitigate their collapse potential during a blast event will depend on the long- and short-term objectives and constraints (both operational and financial) of the tunnel owner/operator.

The following conclusions can be made as a result of the blast analyses in this study:

1. The distribution and magnitude of blast-induced pressure and impulse varies significantly between the two tunnels due to differences in opening size (which influences the standoff from the threat to the ceiling panels and amplifies confinement of the shock wave within the liner). For example, peak pressure in Tunnel 2 (which had the smaller cross-sectional area) for a charge size of 22.7 kg (50 lbs) of TNT equivalent was higher than that in Tunnel 1 under a charge size of 45.4 kg (100 lbs). The maximum impulses, however, are very similar since the blast wave has a very short duration and can still create significant reflections even at lower pressure within the confined tunnel environment.

2. The resistance functions developed from the simplified models provide conservative representations of those obtained from the nonlinear FE models. The tension hangers have low compression capacity and buckle when subjected to upward blast pressure, thus engaging longer panel spans and reducing overall resistance. The simplified models assume several combinations of boundary conditions (with varying rotational restraint and hanger resistance) to bracket the performance of the FE panel models.

3. In a previous study (*8*), the authors determined that typical reinforced concrete liners for roadway tunnels have significant resistance to blast-induced damage (manifested as breach and spall) due to their thickness and the presence of substrate backing (which resists flexure and instead facilitates shock wave propagation through the thickness). The charge sizes needed to cause significant damage and collapse to the drop ceilings are much lower (by approximately one order of magnitude) than those needed to cause substantive damage to the liner. Damage to the ceiling panels without damage to the liner due to modestly sized blast threats can cause catastrophic collapse of the ceiling over much of the tunnel length, thereby posing a significant life safety and operational hazard. Ceiling failure is characterized by significant flexural deformation and shear failure of the concrete panel.

4. Mitigation of blast-induced damage can be achieved via either retrofit or removal of the drop ceiling panel system. For retrofit, FRP reinforcement can be applied via adhesives to the top

surface of the panels (in the plenum) to provide tensile resistance in upward flexure. The hangers must also be upgraded to enable the transfer of elevated upward reactions from the stronger panels. This approach allows the existing ventilation and mechanical systems to remain in place and does not significantly alter the operation of the tunnel. Despite this, FRP retrofit options may only provide enhanced resistance against lower level blast threats with little to no benefit against larger threat sizes that could damage the tunnel liner. In addition, to prevent punching failure, the retrofitted hangers will require local strengthening at the ceiling–to-hanger interface.

5. Removal of the ceiling panels will temporarily reduce operational capacity during demolition and must be accompanied by a replacement or upgrade of the primary ventilation system. With the drop ceiling removed, ventilation will typically be achieved by installing a system of jet fans along the tunnel length. However, removing the ceiling panels not only eliminates their collapse potential during a blast event but also reduces the confinement of the explosion, which can alleviate the resulting pressure and impulse imposed on the tunnel structure.

For the evaluation of drop ceiling under fire demands, the results demonstrate the vulnerability of reinforced concrete drop ceiling panel systems to severe fire in tunnels. Many of these systems are designed only to resist gravity loads (self-weight and a low level of live load) under ambient conditions and are lightweight and long-spanning. Even if the panels survive the material weakening and restraint of thermal expansion during the fire's active heating period, they can still develop a plastic mechanism and potentially fail during cooling due to fire-induced permanent deformations. Tunnels with smaller cross-sections can potentially experience higher temperatures than a larger tunnel for the same fire size due to increased confinement of combustion byproducts and greater proximity to flame radiation (*16*). Fire resistance ratings obtained using standard fire exposures can provide relative quantification of structural robustness, but fire scenarios that include burnout are needed to determine whether the panel will experience post-fire mechanisms when cooling. Panels that remain intact past the end of cooling can then be evaluated for repair or replacement (i.e., for their resilience to fire). The prototype panels considered in this study failed to survive any of the fire scenarios without developing a plastic mechanism and experiencing runaway deflection during either the active heating or subsequent cooling phases. Designers and tunnel owners should consider the duration and maximum intensity of a realistic fire when evaluating the potential for post-fire collapse of these components.

To address the inherent vulnerability of these ceiling systems to fire, three options can be considered as potential mitigation: 1) the fire hazard can be mitigated, 2) the drop ceiling can be hardened or protected, or 3) the ceiling can be removed. Option 1 could be achieved by installing a water mist or deluge fixed firefighting system; however, these systems may not be economically or operationally viable due to the tunnel's location or available resources. Option 2 may be impractical or costly, as significant amounts of fire protection material or additional structural hardening may be needed to provide a significant improvement in structural-fire performance. Fire protection materials used in the tunnel environment would need to be durable, which may preclude the use of conventional spray-on cementitious or gypsum board coatings that are commonly used for passive fire protection in buildings. Option 3 for ceiling removal has become increasingly viable for many tunnels due to recent improvements in the design and implementation of jet fan systems for operational ventilation as well as smoke removal during fire events (*39*, *40*). Also, older drop ceiling systems in tunnels are often removed to reduce maintenance costs, to increase clearance and avoid contact with tall trucks, and to eliminate the risk of falling debris above the roadway surface due to gradual deterioration of the hangers and their anchorages. Even though the

added cost of fan installation would factor into the decision to remove rather than retrofit the drop ceiling, jet fan ventilation systems can potentially offer lower operating and maintenance costs with greater air movement efficiency compared to legacy systems that rely on the plenum above the roadway. The selection of mitigation strategies will be influenced not only by performance objectives (particularly to reduce the risk to motorists and first responders during and after a fire) but also by operational requirements, maintenance considerations, and cost.

References

1. Burch, M. Practical Lessons From Major Accidents: 1999 Alpine Tunnel Fire Killed 39. http://archive.constantcontact.com/fs037/1102467289629/archive/1102628131209.html. Accessed Dec. 17, 2019.
2. USDOT. *Specifications for the National Tunnel Inventory*. Publication No. FHWA-HIF-15-006. U.S. Department of Transportation; Federal Highway Administration, Washington, DC, 2015.
3. Google. Google Maps Street View. https://www.google.com/streetview/.
4. Struzzi, J., and J. Shumway. Why Is PennDOT Removing Squirrel Hill Tunnel's False Ceiling? *CBS Pittsburgh*. https://pittsburgh.cbslocal.com/2012/08/13/why-is-penndot-removing-squirrel-hill-tunnels-false-ceiling/.
5. NTSB. *Ceiling Collapse in the Interstate 90 Connector Tunnel (NTSB/HAR-07/02)*. Publication NTSB/HAR-07/02. National Transportation Safety Board, Washington, DC, 2006.
6. Wallis, S. Tunnel Ceiling Collapse Kills in Japan. https://www.tunneltalk.com/Safety-Dec12-Japan-fatal-tunnel-ceiling-collapse.php. Accessed Mar. 5, 2020.
7. Chung, J. Vintage Photos Show Aftermath of 1960s Explosion That Rocked Delancey Street. *Gothamist News*. http://gothamist.com/2017/01/05/delancey_street_explosion_flashback.php#photo-1.
8. Bai, F., Q. Guo, K. Root, C. Naito, and S. Quiel. Blast Vulnerability Assessment of Road Tunnels with Reinforced Concrete Liners. *Transportation Research Record*, Vol. 2672, No. 41, 2018, pp. 156–164.
9. Maevski, I. *NCHRP Synthesis 415: Design Fires in Road Tunnels–A Synthesis of Highway Practice*. Transportation Research Board, Washington, D.C, 2011.
10. Li, Y. Z. Study of Fire and Explosion Hazards of Alternative Fuel Vehicles in Tunnels. *Fire Safety Journal*, Vol. 110, 2019, p. 102871. https://doi.org/10.1016/j.firesaf.2019.102871.
11. NFPA. *NFPA 502: Standard for Road Tunnels, Bridges, and Other Limited Access Highways*. National Fire Protection Association, Quincy, MA, 2017.
12. Tarada, F., and R. Brandt. Impulse Ventilation for Tunnels – A State of the Art Review. Presented at the 13th Int. Symp. on Aerodynamics and Ventilation of Vehicle Tunnels, New Brunswick, NJ, 2009.
13. Ouyang, Z., A. Carlton, Q. Guo, C. Naito, and S. Quiel. Blast Vulnerability of Drop Ceilings in Roadway Tunnels. *Journal of Performance of Constructed Facilities*, 2020. https://doi.org/10.1061/(ASCE)CF.1943-5509.0001526.
14. NHTSA, (National Highway Traffic Safety Administration). Traffic Safety Facts Annual Report Tables. *Traffic Safety Facts Annual Report Tables*. https://cdan.nhtsa.gov/tsftables/tsfar.htm#. Accessed May 5, 2020.
15. Guo, Q., A. Carlton, S. E. Quiel, and C. J. Naito. Stochastic Thermal Demand and Resulting Capacity Loss of Concrete Tunnel Liners Subjected to Vehicle Fires. *Transportation Research Record*, Vol. 2674, No. 5, 2020, pp. 293–304.
16. Guo, Q., K. J. Root, A. Carlton, S. E. Quiel, and C. J. Naito. Framework for Rapid Prediction of Fire-Induced Heat Flux on Concrete Tunnel Liners with Curved Ceilings. *Fire Safety Journal*, Vol. 109, 2019, p. 102866.

17. Quiel, S. E., T. Yokoyama, L. S. Bregman, K. A. Mueller, and S. M. Marjanishvili. A Streamlined Framework for Calculating the Response of Steel-Supported Bridges to Open-Air Tanker Truck Fires. *Fire Safety Journal*, Vol. 73, 2015, pp. 63–75.
18. ASCE/SEI. *Seismic Evaluation and Retrofit of Existing Buildings (ASCE/SEI 41-13)*. American Society of Civil Engineers, Reston, VA, 2014.
19. Forth, S. Propagation of Shocks in Air (ProSAir) 64. Cranfield University, Shrivenham, UK, , 2018.
20. USACE. Conventional Weapons Effects (ConWep). US Army Corps of Engineers, Vicksburg, MS, , 1992.
21. Century Dynamics. AUTODYN 2D and 3D. Century Dynamics Limited; ANSYS Inc., Fort Worth, TX, , 2005.
22. Rose, T. A. *An Approach to the Evaluation of Blast Loads on Finite and Semi-Infinite Structures*. Doctoral Dissertation. Cranfield University, Cranfield, UK, 2010.
23. LSTC. LS-DYNA. Livermore Software Technology Corporation (LSTC), Livermore, CA, , 2018.
24. ARA. Vulnerability Assessment and Protection Option (VAPO). Applied Research Associates; US Army Corps of Engineers, Raleigh, NC, , 2003.
25. USACE. BLASTX. US Army Corps of Engineers, Vicksburg, MS, , 2007.
26. Stewart, M. G., and M. G. Netherton. Reliability-Based Design Load Factors for Explosive Blast Loading. *Journal of Performance of Constructed Facilities*, Vol. 29, No. 5, 2015, p. B4014010. https://doi.org/10.1061/(ASCE)CF.1943-5509.0000709.
27. Naito, C., and C. Oswald. PCI Design Handbook: Appendix A: Blast-Resistant Design of Precast, Prestressed Concrete Components. *PCI Journal*, Vol. 59, No. 11, 2014, pp. 137–159.
28. PCI. *MNL-141-12: Blast-Resistant Design Manual, 1st Edition*. Precast/Prestressed Concrete Institute, Chicago, IL, 2012.
29. US DOD. *UFC 3-340-02 Structures to Resist the Effects of Accidental Explosions (Including Change 2)*. US Department of Defense, Washington, D.C., 2008.
30. ACI Committee 318. *ACI 318-19: Building Code Requirements for Structural Concrete and Commentary*. American Concrete Institute, Farmington Hills, MI, 2019.
31. Dassault Systèmes. Abaqus 2018. Dassault Systèmes, Vélizy-Villacoublay, France, , 2018.
32. Dassault Systèmes. Abaqus/CAE 2018 User's Guide. Dassault Systèmes, Vélizy-Villacoublay, France, , 2018.
33. Chang, G. A., and J. B. Mander. *NCEER-94-0006: Seismic Energy Based Fatigue Damage Analysis of Bridge Columns: Part I - Evaluation of Seismic Capacity*. Publication NCEER-94-0006. State University of New York, Buffalo, NY, 1994.
34. Alawad, O. *Behavior and Analysis of Blast-Resistant Precast Concrete Wall Panels with Realistic Boundary Conditions and Openings*. Doctoral Dissertation. Lehigh University, Bethlehem, PA, 2019.
35. Alawad, O. M., M. J. Gombeda, S. E. Quiel, and C. Naito. Flexural Performance of Non-Loadbearing Blast-Resistant Precast Concrete Cladding Panels with Discrete Connections. *Journal of Building Engineering*, No. OBE_2019_2562, 2020.
36. Biggs, J. M. *Introduction to Structural Dynamics*. McGraw-Hill, Inc., New York, NY, 1964.
37. PCI Blast and Structural Integrity Committee. Blast Design of Precast / Prestressed Concrete Components. 2009.

38. USACE. *PDC TR 06-08: Single Degree of Freedom Structural Response Limits for Antiterrorism Design*. US Army Corps of Engineers, Protective Design Center, Omaha, NE, 2008.
39. Wang, F., M. Wang, and Q. Wang. Numerical Study of Effects of Deflected Angles of Jet Fans on the Normal Ventilation in a Curved Tunnel. *Tunnelling and Underground Space Technology*, Vol. 31, 2012, pp. 80–85. https://doi.org/10.1016/j.tust.2012.04.009.
40. Yi, L., Q. Xu, Z. Xu, and D. Wu. An Experimental Study on Critical Velocity in Sloping Tunnel with Longitudinal Ventilation under Fire. *Tunnelling and Underground Space Technology*, Vol. 43, 2014, pp. 198–203. https://doi.org/10.1016/j.tust.2014.05.017.
41. AISC. *Steel Construction Manual, 15th Edition (AISC 325-17)*. American Institute of Steel Construction, Chicago, IL, 2017.
42. ACI Committee 440. *ACI 440.2R-17: Guide for the Design and Construction of Externally Bonded FRP Systems for Strengthening Concrete Structures*. American Concrete Institute, Farmington Hills, MI, 2017.
43. Shumway, J. PennDOT To Remove Fort Pitt Tunnel Ceiling. *CBS Pittsburgh*. https://pittsburgh.cbslocal.com/2014/05/15/penndot-to-remove-fort-pitt-tunnel-roof/. Accessed Nov. 24, 2018.
44. Parsons. Appendix C5, Part 2: Tunnel Systems Estimate. In *Interstate 70 Mountain Corridor Traffic and Revenue Study*, Colorado Department of Transportation, Denver, CO.
45. TNO-IBBC. *Beproeving van Het Gedrag Bij Verhitting van Twee Isolatie Materialen Ter Bescherming van Tunnels Bij Brand*. Publication B-79-391. Instituut TNO voor Bouwmaterialen en Bouwconstructies, Delft, the Netherlands, 1979.
46. ASTM. *Test Methods for Determining Effects of Large Hydrocarbon Pool Fires on Structural Members and Assemblies*. ASTM International, West Conshohocken, PA, 2016.
47. National Institute of Standards and Technology (NIST). Consolidated Fire and Smoke Transport (CFAST). National Institute of Standards and Technology (NIST), Gaithersburg, MD, Nov 08, 2019.
48. ASTM Standard E1355-12. *Guide for Evaluating the Predictive Capability of Deterministic Fire Models (Reapproved)*. ASTM International, West Conshohocken, PA, 2018.
49. Peacock, R. D., P. A. Reneke, and G. P. Forney. *CFAST – Consolidated Model of Fire Growth and Smoke Transport (Version 7) Volume 2: User's Guide*. National Institute of Standards and Technology, 2015.
50. Peacock, R. D., P. A. Reneke, and G. P. Forney. *CFAST – Consolidated Model of Fire Growth and Smoke Transport (Version 7) Volume 1: Technical Reference Guide*. Publication NIST TN 1889v1. National Institute of Standards and Technology, 2015, p. NIST TN 1889v1.
51. McGrattan, K., R. McDermott, S. Hostikka, and J. Floyd. *Fire Dynamics Simulator Users Guide, Sixth Edition*. Publication NIST SP 1019. National Institute of Standards and Technology, Gaithersburg, MD, 2013.
52. Li, Y. Z., C. Huang, J. Anderson, R. Svensson, H. Ingason, B. Husted, M. Runefors, and J. Wahlqvist. *Verification, Validation and Evaluation of FireFOAM as a Tool for Performance Design*. Lund University, Lund, Sweden, 2017.
53. Ingason, H. Design Fire Curves for Tunnels. *Fire Safety Journal*, Vol. 44, No. 2, 2009, pp. 259–265.
54. Iqbal, N., M. H. Salley, and S. Weerakkody. *NUREG-1805 "Fire Dynamics Tools (FDTs): Quantitative Fire Hazard Analysis Methods for the U.S. Nuclear Regulatory Commission Fire Protection Inspection Program" (Final Report).* Division of System Safety and Analysis

Office of Nuclear Reactor Regulation U.S. Nuclear Regulatory Commission Washington, DC 20555-0001, Washington, D.C, 2004, p. 1016.
55. Carvel, R. O., A. N. Beard, P. W. Jowitt, and D. D. Drysdale. Variation of Heat Release Rate with Forced Longitudinal Ventilation for Vehicle Fires in Tunnels. *Fire Safety Journal*, Vol. 36, No. 6, 2001, pp. 569–596. https://doi.org/10.1016/S0379-7112(01)00010-8.
56. Li, Y. Z., C. G. Fan, H. Ingason, A. Lönnermark, and J. Ji. Effect of Cross Section and Ventilation on Heat Release Rates in Tunnel Fires. *Tunnelling and Underground Space Technology*, Vol. 51, 2016, pp. 414–423. https://doi.org/10.1016/j.tust.2015.09.007.
57. Ingason, H., Y. Z. Li, and A. Lönnermark. *Runehamar Tunnel Fire Tests (SP Report 2011:55)*. Publication SP Report 2011:55. SP Technical Research Institute of Sweden, Boras, Sweden, 2011.
58. Haddad, R. K., C. Maluk, E. Reda, and Z. Harun. Critical Velocity and Backlayering Conditions in Rail Tunnel Fires: State-of-the-Art Review. *Journal of Combustion*. Volume 2019, e3510245. https://www.hindawi.com/journals/jc/2019/3510245/. Accessed Jul. 28, 2020.
59. Li, Y. Z., and H. Ingason. Position of Maximum Ceiling Temperature in a Tunnel Fire. *Fire Technology*, Vol. 50, No. 4, 2014, pp. 889–905. https://doi.org/10.1007/s10694-012-0309-2.
60. Franssen, J.-M., and T. Gernay. Modeling Structures in Fire with SAFIR ®: Theoretical Background and Capabilities. *Journal of Structural Fire Engineering*, Vol. 8, No. 3, 2017, pp. 300–323.
61. CEN. *EN 1992-1-2: Eurocode 2: Design of Concrete Structures - Part 1-2: General Rules - Structural Fire Design*. European Commission for Standardization, Brussels, Belgium, 2008.
62. García, E., A. de Pablos, M. A. Bengoechea, L. Guaita, M. I. Osendi, and P. Miranzo. Thermal Conductivity Studies on Ceramic Floor Tiles. *Ceramics International*, Vol. 37, No. 1, 2011, pp. 369–375. https://doi.org/10.1016/j.ceramint.2010.09.023.
63. CEN. *EN 1991-1-2:2002 Eurocode 1: Actions on Structures - Part 1-2: General Actions - Actions on Structures Exposed to Fire*. European Committee for Standardization, Brussels, Belgium, 2009.
64. Maevski, I., National Cooperative Highway Research Program, Transportation Research Board, and National Academies of Sciences, Engineering, and Medicine. *Guidelines for Emergency Ventilation Smoke Control in Roadway Tunnels*. Transportation Research Board, Washington, D.C., 2017.
65. Chávez-Galán, J., R. Almanza, and N. R. Cuevas. Convective Heat Transfer Coefficients: Experimental Estimation and Its Impact on Thermal Building Design for Walls Made of Different Mexican Building Materials. *Concreto y Cemento. Investigación y Desarrollo*, Vol. 5, No. 2, 2014, p. 13.
66. Montazeri, H., and B. Blocken. New Generalized Expressions for Forced Convective Heat Transfer Coefficients at Building Facades and Roofs. *Building and Environment*, Vol. 119, 2017, pp. 153–168. https://doi.org/10.1016/j.buildenv.2017.04.012.
67. Quiel, S., and M. Garlock. Parameters for Modeling a High-Rise Steel Building Frame Subject to Fire. *Journal of Structural Fire Engineering*, Vol. 1, No. 2, 2010, pp. 115–134. https://doi.org/10.1260/2040-2317.1.2.115.
68. ASCE/SEI. *Minimum Design Loads for Buildings and Other Structures (ASCE/SEI 7-16)*. American Society of Civil Engineers, Reston, VA, 2017.

69. Elghazouli, A. Y., K. A. Cashell, and B. A. Izzuddin. Experimental Evaluation of the Mechanical Properties of Steel Reinforcement at Elevated Temperature. *Fire Safety Journal*, Vol. 44, No. 6, 2009, pp. 909–919. https://doi.org/10.1016/j.firesaf.2009.05.004.
70. CEN. *EN 1994-1-2:2005 Eurocode 4: Design of Composite Steel and Concrete Structures - Part 1-2: General Rules - Structural Fire Design*. European Committee for Standardization, Brussels, Belgium, 2008.
71. Gernay, T., and J.-M. Franssen. A Formulation of the Eurocode 2 Concrete Model at Elevated Temperature That Includes an Explicit Term for Transient Creep. *Fire Safety Journal*, Vol. 51, 2012, pp. 1–9. https://doi.org/10.1016/j.firesaf.2012.02.001.
72. Gernay, T. Effect of Transient Creep Strain Model on the Behavior of Concrete Columns Subjected to Heating and Cooling. *Fire technology*, Vol. 48, No. 2, 2012, pp. 313–329.
73. Ni, S., and T. Gernay. Predicting Residual Deformations in a Reinforced Concrete Building Structure after a Fire Event. *Engineering Structures*, Vol. 202, 2020, p. 109853. https://doi.org/10.1016/j.engstruct.2019.109853.
74. ASTM Standard E119-20. *Test Methods for Fire Tests of Building Construction and Materials*. ASTM International, West Conshohocken, PA, 2020.
75. Hertz, K. D. Limits of Spalling of Fire-Exposed Concrete. *Fire Safety Journal*, Vol. 38, No. 2, 2003, pp. 103–116. https://doi.org/10.1016/S0379-7112(02)00051-6.
76. Choi, S.-W., J. Lee, and S.-H. Chang. A Holistic Numerical Approach to Simulating the Thermal and Mechanical Behaviour of a Tunnel Lining Subject to Fire. *Tunnelling and Underground Space Technology*, Vol. 35, 2013, pp. 122–134. https://doi.org/10.1016/j.tust.2013.01.004.
77. Yan, Z., H. Zhu, J. Woody Ju, and W. Ding. Full-Scale Fire Tests of RC Metro Shield TBM Tunnel Linings. *Construction and Building Materials*, Vol. 36, 2012, pp. 484–494. https://doi.org/10.1016/j.conbuildmat.2012.06.006.
78. Zhang, Q., W. Wang, S. Bai, and Y. Tan. Response Analysis of Tunnel Lining Structure under Impact and Fire Loading. *Advances in Mechanical Engineering*, Vol. 11, No. 3, 2019, p. 168781401983447. https://doi.org/10.1177/1687814019834473.
79. Ali, F., A. Nadjai, and A. Abu-Tair. Explosive Spalling of Normal Strength Concrete Slabs Subjected to Severe Fire. *Materials and Structures*, Vol. 44, No. 5, 2011, pp. 943–956. https://doi.org/10.1617/s11527-010-9678-5.

Appendix A: Technology Transfer Activities

1 Accomplishments

An extensive numerical evaluation of tunnel drop ceilings under blast and fire loading was conducted. ProSAir and general SDOF method were employed to develop a deeper understanding of the failure mechanisms that develop in response to close-in blast loading. CFAST and SAFIR were adopted to generate the spatial temperature distribution in tunnels and failure mechanism of drop ceiling panels after exposed to high temperature. Parameters effecting damage for a given charge size and fire size were numerically evaluated: backfill material/fuel type, liner thickness and strength.

1.1 What was done? What was learned?

For drop ceilings under blast demands:

- The distribution and magnitude of blast-induced pressure and impulse varies significantly between the two tunnels due to differences in opening size (which influences the standoff from the threat to the ceiling panels and amplifies confinement of the shock wave within the liner). For example, peak pressure in Tunnel 2 (which had the smaller cross-sectional area) for a charge size of 22.7 kg (50 lbs) of TNT equivalent was higher than that in Tunnel 1 under a charge size of 45.4 kg (100 lbs). The maximum impulses, however, are very similar since the blast wave has a very short duration and can still create significant reflections even at lower pressure within the confined tunnel environment.
- The resistance functions developed from the simplified models provide conservative representations of those obtained from the nonlinear FE models. The tension hangers have low compression capacity and buckle when subjected to upward blast pressure, thus engaging longer panel spans and reducing overall resistance. The simplified models assume several combinations of boundary conditions (with varying rotational restraint and hanger resistance) to bracket the performance of the FE panel models.
- In a previous study (*8*), the authors determined that typical reinforced concrete liners for roadway tunnels have significant resistance to blast-induced damage (manifested as breach and spall) due to their thickness and the presence of substrate backing (which resists flexure and instead facilitates shock wave propagation through the thickness). The charge sizes needed to cause significant damage and collapse to the drop ceilings are much lower (by approximately one order of magnitude) than those needed to cause substantive damage to the liner. Damage to the ceiling panels without damage to the liner due to modestly sized blast threats can cause catastrophic collapse of the ceiling over much of the tunnel length, thereby posing a significant life safety and operational hazard. Ceiling failure is characterized by significant flexural deformation and shear failure of the concrete panel.
- Mitigation of blast-induced damage can be achieved via either retrofit or removal of the drop ceiling panel system. For retrofit, FRP reinforcement can be applied via adhesives to the top surface of the panels (in the plenum) to provide tensile resistance in upward flexure. The hangers must also be upgraded to enable the transfer of elevated upward reactions from the stronger panels. This approach allows the existing ventilation and mechanical systems to remain in place and does not significantly alter the operation of the tunnel. Despite this, FRP retrofit options may only provide enhanced resistance against lower level blast threats with little to no benefit against larger threat sizes that could damage the tunnel liner. In

addition, to prevent punching failure, the retrofitted hangers will require local strengthening at the ceiling–to-hanger interface.

- Removal of the ceiling panels will temporarily reduce operational capacity during demolition and must be accompanied by a replacement or upgrade of the primary ventilation system. With the drop ceiling removed, ventilation will typically be achieved by installing a system of jet fans along the tunnel length. However, removing the ceiling panels not only eliminates their collapse potential during a blast event but also reduces the confinement of the explosion, which can alleviate the resulting pressure and impulse imposed on the tunnel structure.

For drop ceilings under blast demands:

- Even if the panels survive the material weakening and restraint of thermal expansion during the fire's active heating period, they can still develop a plastic mechanism and potentially fail during cooling due to fire-induced permanent deformations. Tunnels with smaller cross-sections can potentially experience higher temperatures than a larger tunnel for the same fire size due to increased confinement of combustion byproducts and greater proximity to flame radiation (*16*). Fire resistance ratings obtained using standard fire exposures can provide relative quantification of structural robustness, but fire scenarios that include burnout are needed to determine whether the panel will experience post-fire mechanisms when cooling. Panels that remain intact past the end of cooling can then be evaluated for repair or replacement (i.e., for their resilience to fire). The prototype panels considered in this study failed to survive any of the fire scenarios without developing a plastic mechanism and experiencing runaway deflection during either the active heating or subsequent cooling phases. Designers and tunnel owners should consider the duration and maximum intensity of a realistic fire when evaluating the potential for post-fire collapse of these components.
- To address the inherent vulnerability of these ceiling systems to fire, three options can be considered as potential mitigation: 1) the fire hazard can be mitigated, 2) the drop ceiling can be hardened or protected, or 3) the ceiling can be removed. Option 1 could be achieved by installing a water mist or deluge fixed firefighting system; however, these systems may not be economically or operationally viable due to the tunnel's location or available resources. Option 2 may be impractical or costly, as significant amounts of fire protection material or additional structural hardening may be needed to provide a significant improvement in structural-fire performance. Fire protection materials used in the tunnel environment would need to be durable, which may preclude the use of conventional spray-on cementitious or gypsum board coatings that are commonly used for passive fire protection in buildings. Option 3 for ceiling removal has become increasingly viable for many tunnels due to recent improvements in the design and implementation of jet fan systems for operational ventilation as well as smoke removal during fire events (*39*, *40*).
- Older drop ceiling systems in tunnels are often removed to reduce maintenance costs, to increase clearance and avoid contact with tall trucks, and to eliminate the risk of falling debris above the roadway surface due to gradual deterioration of the hangers and their anchorages. Even though the added cost of fan installation would factor into the decision to remove rather than retrofit the drop ceiling, jet fan ventilation systems can potentially offer lower operating and maintenance costs with greater air movement efficiency compared to legacy systems that rely on the plenum above the roadway. The selection of

mitigation strategies will be influenced not only by performance objectives (particularly to reduce the risk to motorists and first responders during and after a fire) but also by operational requirements, maintenance considerations, and cost.

1.2 How have the results been disseminated?

- The results were presented at 1) *Tunneling Fundamentals, Practice and Innovations Short Course*, Colorado School of Mines, Golden, October 2019; 2) *Webinar Series from University Transportation Center for Underground Transportation Infrastructure*, December 2019; 3) *Poster Session of TRB 100th Annual Meeting*, January 2021.

- Two journal papers have been published based on the result, including ASCE Journal of Performance of Constructed Facilities, Transportation Research Record.

2 Participants and Collaborating Organizations

Name: Lehigh University

Location: Bethlehem, PA

Contribution: (1) The demands of peak pressure and impulse of three charge sizes of TNT were determined by ProSAir. (2) The failure and damage of drop ceiling panels under blast demands were analyzed for two prototype tunnels. (4) The demands of temperature of three sizes of natural fire from gasoline were determined by SAFIR. (4) The collapse mechanism of drop ceiling panels under natural fire and standard fire were analyzed for two prototype tunnels. (5) The recommendations of tunnel rehabilitation to improve tunnel fire and blast resistance were given.

3 Outputs

Journal publications

- Ouyang, Z., A. Carlton, Q. Guo, C. Naito, and S. Quiel. Blast Vulnerability of Drop Ceilings in Roadway Tunnels. Journal of Performance of Constructed Facilities, 2020. https://doi.org/10.1061/(ASCE)CF.1943-5509.0001526.

- Ouyang Z, Guo Q, Quiel SE, Naito CJ. Vulnerability of Drop Ceilings in Roadway Tunnels to Fire-Induced Damage. Transportation Research Record. 2021;2675(11):1400-1412. doi:10.1177/03611981211026659

Workshops and Presentations

- Ziyan Ouyang "Blast Vulnerability of Drop Ceilings in Roadway Tunnels" at *Tunneling Fundamentals, Practice and Innovations Short Course*, Colorado School of Mines, Golden, October 2019.

- Clay Naito, "Blast Vulnerability of Drop Ceilings in Roadway Tunnels" at *Webinar Series from University Transportation Center for Underground Transportation Infrastructure*, December 2019.

- Ziyan Ouyang, "Vulnerability of Drop Ceilings in Roadway Tunnels to Fire-Induced Damage", *Poster Session of TRB 100th Annual Meeting*, January 2021.

4 Outcomes

- The behavior of concrete drop ceiling subjected to blast and fire can be analytically and numerically studied.
- The simplified general SDOF approach can give an appropriate estimation of structural resistance with various boundary conditions.
- The equivalent gasoline fire is proposed for vehicle fire modelling as a simplification of the various materials on the vehicle which result in complex combustion behaviors. The HRR is used as the key factor to represent the intensity of the fire. Current standard temperature curves of fire testing can be a conservative tool to assess the fire performance.
- Drop ceilings can generally survive during intensive fire events, but it can collapse during cooling phase after due to material degradation and tension force developed.

5 Impacts

- The performance of major structural components, other than tunnel liner, under fire and blast was assessed. Based on current technology of ventilation system, the tunnel drop ceilings can be eliminated for new tunnel construction. From analyses and recent tunnel rehabilitation projects, the simplest way to improve the overall tunnel fire and blast performance of the tunnels equipped with drop ceilings is to remove the drop ceilings.

Appendix B: Data from the Project

Concrete and Steel Models in FE Analyses

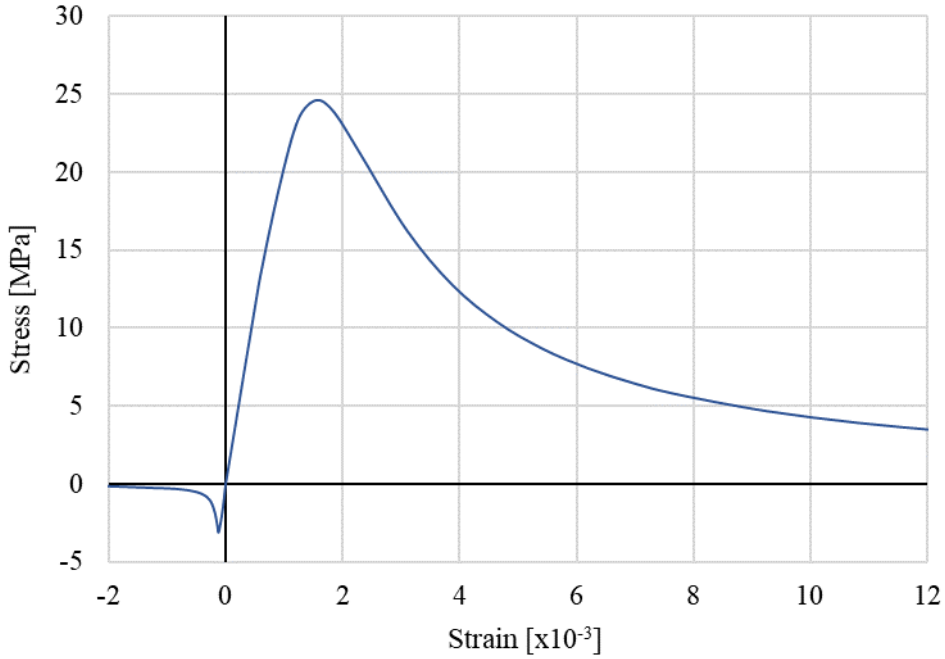

Fig. 27: Concrete stress-strain model in finite element analyses

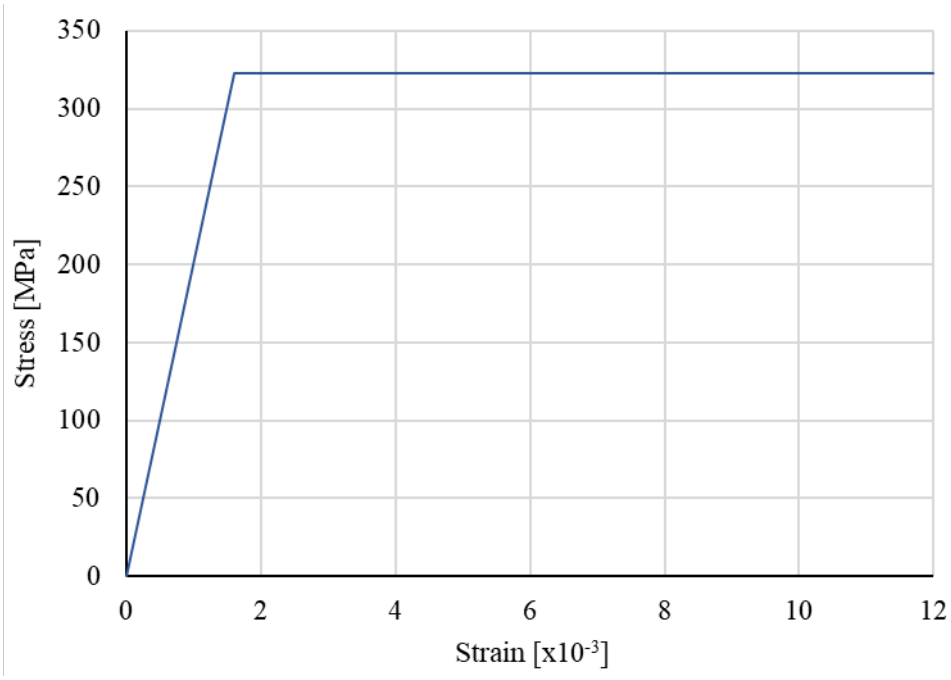

Fig. 28: Steel stress-strain model in finite element analyses

PROSAIR input file example

```
[General]
nr_of_threads=4
output_velocities=1
delay_target_output=1
move_bad_targets=1
split_target_files=0
white_background=1
check_prefix=check
check_interval=0
check_end_phase=1
switch_time=0.0012
atmos_pressure=101325
atmos_temperature=284
[Explosive]
type=TNT
mass=22.6796
[Materials]
additional_dir=C:\\Users\\aec518\\Desktop\\Research\\ProSAir\\500lbs-ORtunnel\\Materials
[Spherical]
execute=1
domain_radius=0.6096
cell_size=0.001501
adjust_dr_to_charge=1
max_time=1
cfl=0.75
boundary_r=0
display_interval=100
plot_variable=5
store_plots=0
draw_targets=1
[Cylindrical]
execute=0
height_of_blast=0
rmax=3.6576
hmax=4.2672
cell_size=0.3048
```

boundary_r=0
boundary_h=0
max_time=1
cfl=0.75
display_interval=50
display_plane=2
plotting_planes=3.6576, 4.2672
plot_variable=5
scale_factor=1
store_plots=0
draw_targets=1
[3d]
execute=1
origin_of_blast=8.0104, 152.629, 1.6096
xmin=0
xmax=16.0208
ymin=0
ymax=305.258
zmin=0
zmax=9.382
cell_size=0.1524
boundary_xmin=1
boundary_xmax=1
boundary_ymin=1
boundary_ymax=1
boundary_zmin=1
boundary_zmax=1
display_plane=3
plotting_planes=0, 0, 0
max_time=1
cfl=0.5
display_interval=10
skip_final_checkpoint=0
plot_variable=5
store_plots=0
scale_factor=1
draw_targets=1

target_0=8.0104:8.0104:1,0:152.4:26,6.94359:6.94359:1

target_1=9.763:9.763:1,0:152.4:26,6.94359:6.94359:1

target_2=11.5156:11.5156:1,0:152.4:26,6.94359:6.94359:1

target_3=12.3538:12.3538:1,0:152.4:26,6.94359:6.94359:1

obstacle_0=cuboid;0 1 0 305.258 0 9.382;Solid

obstacle_1=cuboid;1.0001 15.0207 0 305.258 0 1;Solid

obstacle_2=cuboid;15.0208 16.0208 0 305.258 0 9.382;Solid

obstacle_3=cuboid;1.001 15.0207 0 305.258 6.9436 7.9436;Solid

obstacle_4=wedge;1.001 0 4.9436 1.001 0 6.9435 2.524 0 6.9435 305.258 y;Solid

obstacle_5=wedge;15.0207 0 4.9436 13.4968 0 6.9435 15.0207 0 6.9435 305.258 y;Solid

General SDOF Anlyses example